

Construction of a 10-min-gridded precipitation data set for the Greater Alpine Region for 1800–2003

Dimitrios Efthymiadis, Philip D. Jones, and Keith R. Briffa

Climatic Research Unit, School of Environmental Sciences, University of East Anglia, Norwich, UK

Ingeborg Auer, Reinhard Böhm, and Wolfgang Schöner

Central Institute for Meteorology and Geodynamics, Vienna, Austria

Christoph Frei

MeteoSwiss, Zurich, Switzerland

Jürg Schmidli

Institute for Atmospheric and Climate Science, ETH, Zurich, Switzerland

An edited version of this paper was published by AGU. Copyright [2006] American Geophysical Union.

Citation: Efthymiadis, D., P. D. Jones, K. R. Briffa, I. Auer, R. Böhm, W. Schöner, C. Frei, and J. Schmidli (2006), Construction of a 10-min-gridded precipitation data set for the Greater Alpine Region for 1800–2003, *Journal of Geophysical Research*, 110, D01105, doi:10.1029/2005JD006120.

Abstract

1. Introduction

2. Data and Preprocessing

2.1. HISTALP station-mode (1800–2003)

2.2. ETH Climatology (1971–1990)

2.3. Extensions of the ETH Climatology to the Whole GAR

2.4. ETH Monthly (1901–1990)

2.5. CRU TS 2.0 Monthly (1901–2000)

2.6. MeteoSwiss Monthly (1961–2000)

2.7. CHCAM Monthly (1951–2000)

3. Gridding Interpolation Scheme

3.1. Reconstruction of Incomplete Station Series

3.2. Data interpolation

3.3. Interpolated Field Accuracy

4. Evaluation of the Gridded Precipitation Data Set

4.1. Correlation Analysis

4.2. Multi-decadal Trends

4.3. Cases of Excessive Precipitation

4.4. Remaining Uncertainties

5. Conclusions

Appendix A

Appendix B

Acknowledgements

References

Tables

Figures

Abstract

A new precipitation data set for the Greater Alpine Region (GAR; 4°E–19°E, 43°N–49°N) has been developed. It provides monthly precipitation totals, for the 1800–2003 period, gridded at 10-minute resolution. The new HISTALP 10-min-grid data set is based on 192 long-term homogenized precipitation series from meteorological stations across the study domain and a high-resolution precipitation climatology for the 1971–1990 period. The effective coverage of the data set depends on the observations available in the station network which progressively declines back to the early 19th century (from 192 to 5 stations). To aid the use of these data in other studies, an accompanying data set has also been developed, which provides a measure of the quality of each monthly precipitation estimate over the grid: the explained variance, relative to the 1931–2000 (maximum data availability) period. The computed quality score illustrates the comparatively poorer accuracy of the data set for regions and months with less coherent precipitation fields (i.e., over the Alps and in summer) and when the number of stations is reduced, particularly before 1840. The derived gridded field has also been compared for the whole and geographical sub-regions with other independently-developed data sets and is found to provide a similar description of the precipitation in the GAR for places and periods of common coverage. The data set is publicly available at <http://www.cru.uea.ac.uk/>.

1. Introduction

The precipitation field of the European Alps is perhaps both the best observed and most studied among the topographically and climatically complex regions of the Earth. A comprehensive listing of the many studies can be found in *Frei and Schär*, [1998]. These studies have benefited from a network of meteorological stations, which operated in the area with its maximum density during the second half of the 20th century. This network enabled the construction of gridded climatologies and multidecadal data sets with grid resolution of ~100 m to ~100 km, at a daily to annual temporal resolution (see Table 1). The construction of these data sets was carried out either for individual national territories, or transnational domains, and in some cases were part of global-scale studies. None of the gridded data sets constructed to date, however, extends before 1901 constraining the length and timescale of climatic variations that can be considered.

A multicentury description of precipitation is necessary to achieve an extended understanding of the climate variability in the Greater Alpine Region (GAR, 4–19°E, 43–49°N; see Figure 1) with particular emphasis on its long-term components. This need has recently led to the development of meteorological records from various international, national and sub-national instrumental data collections and the construction of a new data set with long-term, homogenized time series of monthly precipitation totals for 192 sites in the GAR [*Auer et al.*, 2005]. A few of the time series extend back to 1800, whereas most of them start within the 19th century. Complete data coverage is provided from 1927 to 2003. This data set is part of a general climatic database in development, named “HISTALP”, which comprises instrumental monthly climate time series for the realm of the European Alps. Its development began in the early 1990s with single long-term variable data sets for Austria (e.g., *Böhm*, [1992] for temperature; *Auer*, [1993] for precipitation). Later, *Auer et al.*, [2001a] developed a multiple Austrian data set for 9 climate variables. Since then, intensification of the collaboration of all climate data providers for the region has allowed an extension to the recent target region of HISTALP (the GAR). The quality requirements follow a list of principles which are regarded as essential for climate variability research in the instrumental period. Full exploitation of the data potential is achieved with respect to: (1) duration (reaching far enough into the early instrumental period when anthropogenic forcing was weak), (2) spatial and temporal resolution (meeting the demands with respect to the correlation length scales in space and time), (3) multi-variable (several, at least the main climate variables: temperature, precipitation, mean sea level pressure), (4) data quality in terms of homogeneity (non-climatic breaks removed, non-climatic trends detected and at least flagged), and (5) data quality in terms of outlier detection and elimination.

The final version of HISTALP will be based on station time series (original and homogenised in absolute values) in a gridded form (anomaly series at 1 deg lat.–lon. resolution) and at a higher-resolution gridded form (absolute gridded fields with resolution appropriate to the respective climate element). The HISTALP database development is described by I. Auer et al. (manuscript submitted to *International Journal of Climatology*, 2005). So far, precipitation (monthly totals) is the first variable to be thoroughly studied.

Schöner [2004] has developed the HISTALP standard-grid version of the precipitation data set, which consists of monthly anomaly series (ratios) relative to the respective 20th century averages at a spatial resolution of 1 deg in latitude and longitude, respectively. The gridding method used was first applied by *Auer and Böhm* [1994] to the Austrian long-term temperature and precipitation series described in *Böhm* [1992] and *Auer* [1993] and was extended, with slight changes, to the GAR. For the interpolation of HISTALP station data, a Gaussian-shaped inverse distance weighting function was used, with half weight at 100 km distance from the grid-point and zero weight beyond 150 km. In particular, to avoid mixing of incoherent precipitation regions, extrapolation of values from sites separated by the main orographic divide through the Alps and the Dinaric mountain chains was not allowed. As the study region shows a homogeneous coverage with climate stations, an angular weighting approach was not used for interpolation of HISTALP standard-grid version.

The processing of the HISTALP higher-resolution-gridded precipitation data set is the topic of this paper. The data set being developed comprises time series of monthly totals, on a regular 10-minute grid over the GAR, spanning the period 1800 to 2003. The data set construction is intended to facilitate grid-based multi-parameter studies of Alpine climate, to validate numerical models, and to calibrate climatic proxies which are not always located nearby meteorological sites. Hereafter, the station-based homogenized precipitation extract from the HISTALP database will be referred to as ‘HISTALP station-mode’ and the higher-resolution data set as ‘HISTALP 10-min-grid’. Section 2 of the paper outlines the various data sets used, section 3 describes the gridding method, section 4 evaluates the resulting data set and section 5 concludes.

2. Data and Preprocessing

Various data sets were used for developing and evaluating the new data set. The ‘development data sets’ are described in sections 2.1–2.3 and the ‘evaluation data sets’ in sections 2.4–2.7. The description of the data sets includes an overview of their characteristics and mentions how they are used. An overall summary is provided in Table 2.

2.1. HISTALP station-mode (1800–2003)

The number of available precipitation series from the HISTALP station-mode data set increases from 1800 to 1927 (Figure 2). The mean inter-station distance (i.e. the mean value of the distance between each station and its nearest neighbor) gradually decreases from ~ 224 km (5 stations) in 1800 to ~ 38 km (192 stations) during the 1927–2003 period. The most recent time series (starting during the 20th century) are mainly from Switzerland and NW Italy. However, at the regional scale, it is the Croatia and Bosnia–Herzegovina region which has the shortest time series; in parts the time series only start in the 1860s/1880s. The homogenization adjustments (detailed in *Auer et al.*, [2005]) applied to the data set aimed to improve the data quality, and in particular to account for the breaks and non-climatic outliers detected in the time series. To underline the necessity of a careful consideration of breaks in homogeneity and outlier detection and elimination (e.g., issues that have to and can be avoided) we note that in the 192 station series of an average length of 138 years more than 900 breaks and more than 500 erroneous outliers could be located and adjusted. The inhomogeneities were not random but would have caused biases in larger sub-regions and also for the entire GAR. The outliers would have considerably compromised any future studies of extreme events. Finally, the missing data (~10% missing data rate for the first seven decades of the 19th century and less than 5% afterwards, except for the period of the two world wars) were filled in by estimates from highly-correlated comparative series. The HISTALP station-mode data set is considered reliable back to 1840, whereas it provides the best that can be currently achieved for the first four decades of the 19th century, given the availability of gauge data and metadata (station information). This data set is the basic source for the gridded precipitation data set development.

2.2. ETH Climatology (1971–1990)

This monthly precipitation climatology data set based on the 20-year period 1971–1990 was also used. It has been developed from the doctoral work of *Schwarb* [2000] at the Swiss Federal Institute of Technology (ETH) in Zurich, also published as part of the Hydrological Atlas of Switzerland (HADES) [*Schwarb et al.*, 2001]. The original data set was developed by spatially analyzing quality-controlled rain-gauge observations (~ 6090 time series, see Figure 3a, including 250 time series from monthly rain gauges located at high elevations) across the GAR and interpolating onto a regular grid of 1.25 min × 1.25 min resolution (1.6 km × 2.3 km); each grid-cell value represents the area-mean precipitation for every calendar month. The distribution of stations analyzed is fairly balanced over the northern and western portions of the analysis domain, while the coverage is more variable for the southern region

(particularly over parts of Italy). A modified/calibrated version of the PRISM technique [Daly *et al.*, 1994, 2002] was implemented for the interpolation of mean monthly totals at the stations onto a regular grid. For the needs of our study a 10 min × 10 min gridded climatology (hereafter ‘ETH climatology’) was obtained by spatially averaging the original high-resolution climatology. The ETH climatology (see Figure 3b for the annual mean field) will be necessary for calculating later the absolute grid-based series after the interpolation of percentage (anomaly) station series (see section 3.2).

2.3. Extensions of the ETH Climatology to the Whole GAR

As the ETH climatology does not completely cover the eastern territory of our study area, additional data from the Czech Republic, Slovakia, Hungary, Croatia, Bosnia-Herzegovina, and central Italy were selected and analyzed to construct a regional climatology there. Four categories of data were blended:

- a) Marginal ETH data from Central Italy, Germany, Austria, Slovenia and Croatia.
- b) Twenty HISTALP station time series for the period 1971–1990
- c) GHCN station time series [Vose *et al.*, 1992]; missing data in the 1971–1990 period were filled in with reconstructed values using HISTALP station-mode data from nearby stations (see section 3.1)
- d) Various station climatic normals (i.e., mean precipitation, for each calendar month, over a certain multiyear period) from the CRU databank. Since most of them refer to the 1961–1990 period, they were re-adjusted to 1971–1990 using the 1971–1990 to 1961–1990 ratios of monthly averages of nearby HISTALP stations. To increase the confidence in the estimated values, the median, among those derived using the three nearest HISTALP time series, was selected.

The geographical locations of the stations which supplied the additional data are given in Figure 3b.

All the above data were interpolated using thin-plate smoothing splines [Wahba, 1979; Hutchinson, 1995]. Spline interpolation was selected because it is more robust in areas with sparse or irregularly spaced data points. It was implemented using the ANUSPLIN software developed by Mike Hutchinson at the Australian National University [Hutchinson, 2000]. Different weights were assigned to each category of data, with the maximum corresponding to the ETH data, whereas for the other sources, weights varied according to the proportion of temporal coverage of the original station data (before reconstruction or adjustment) based on the 1971–1990 period.

The annual mean of the complete GAR climatology (1971–1990) is shown in Figure 3c. It should be noted that in areas where the climatology augmentation took place the resultant field is not as accurate as the ETH climatology, since the sparseness of the stations available did not allow the estimation of the true area-mean precipitation for each grid cell.

2.4. ETH Monthly (1901–1990)

This ETH data set covers the region of the European Alps (3.2–16.2°E, 43.2–48.8°N) for the 1901–1990 period with monthly precipitation totals over a grid with spacing of 0.30° long × 0.22° lat (spatial resolution of ~25 km). There are 928 time series, in total, each one of them corresponding to a specific grid point. The ETH precipitation data set results from the work of Schmidli *et al.* [2001, 2002], who analyzed, using EOFs, a gridded monthly precipitation data set [Frei and Schär, 1998] corresponding to a recent, densely-observed period (~6800 rain-gauge stations, 1971–1990) and then used the spatial EOFs to reconstruct the precipitation field of previous, sparsely-observed (140 stations; see Figure 4a) decades earlier in the 20th century. A reduced-space interpolation technique [Kaplan *et al.*, 1997] was used to develop the reconstruction. The purpose of this approach was to recover mesoscale patterns of precipitation variability that are not resolved in the sparse long-term network but contained in the high-resolution space-time variations over a recent period. The ETH monthly data set is used for evaluating the new data set.

2.5. CRU TS 2.0 Monthly (1901–2000)

The CRU TS 2.0 data set (just ‘CRU’ hereafter) provides the precipitation field (together with other climatic parameters) for global land areas and several rain gauge-equipped islands over an equal-distance grid of $0.5^\circ \times 0.5^\circ$. The corresponding spatial resolution in the Alpine region is $\sim 39 \times 56$ km, in longitude and latitude, respectively. It comprises time series of monthly precipitation totals from 1901 to 2000.

The CRU data set was produced by *Mitchell et al.*, [2004]. It is an updated version of earlier work [*New et al.*, 1999, 2000] and utilizes the multi-source CRU databases of station observations. An angular distance-weighted (ADW) interpolation was used for averaging precipitation anomalies from the eight nearest stations to each grid point. The interpolated precipitation anomalies were expressed as a percentage of the 1961–1990 mean field. The station data availability used for the geographical window of the GAR, varied throughout the 20th century reaching its maximum during the 1960–1987 period (see Figure 4b). The time series of the CRU data set are used for evaluating the new HISTALP 10-min-grid precipitation data set.

2.6. MeteoSwiss Monthly (1961–2000)

A data set of 439 time series from Swiss stations was provided by MeteoSwiss, which spans the 1959–2000 period. Missing values in station time series were in some cases filled by “synthetic data” from old nearby stations after adapting them to the measuring conditions of the new sites by homogenization (Michael Begert, personal communication). As a result, 325 continuously cover the 1961–2000 interval (Figure 5a). The MeteoSwiss data set is used to define the weighting function for the interpolation of anomalies (the ‘radial’ term; see section 3), and for examining the accuracy of the HISTALP 10-min-grid data set for months with extreme precipitation (see section 4.3). Although the conclusions derived refer to Swiss-specific meteorological conditions, the combination of contrasting high spatial coherent precipitation in the northwest and pronounced low coherence in the southeast part of Switzerland makes this region suitable for studying the precipitation field in a mountainous terrain, with a spatially dense observational network.

2.7. CHCAM Monthly (1951–2000)

Gyalistras [2003] developed a data set describing the precipitation field on a ~ 5 km \times 5 km grid ($0.05^\circ \times 0.05^\circ$) for Switzerland. It consists of the 1961–1990 mean fields (i.e. climatology, referred as CHCM), plus the monthly anomaly fields for the 1951–2000 period (CHCAM hereafter). For the development of the climatology, 515 MeteoSwiss station time series were analyzed, whereas, due to the shorter availability of complete data in 1951–2000, only 147 station time series were used for the anomaly maps (Figure 5b). A sophisticated interpolation method was implemented, which took into account the multiscale relationship of precipitation with the geographical location, elevation and time (calendar month) of the year (see [*Gyalistras*, 2003] for details). The high-resolution anomaly data set is used for validating the comparatively coarser HISTALP 10-min-grid data set developed in the present study (see section 4).

3. Gridding Interpolation Scheme

The gridding scheme follows the “anomaly approach” [e.g., *Jones et al.*, 1982; *Jones and Hulme*, 1996] which is based on the characteristics of the two components of the field: the long-term time-mean component (the “climatology”) and the temporal deviations from this (the “anomalies”). The time-mean component is more strongly tied to the physiography (mainly the orography for precipitation) of a geographical domain, and may exhibit small-scale discontinuities in space. However, since it is quite stable in time, it can be estimated using a dense station network for a period which does not necessarily

have to be long. This is the case with the station data availability in the GAR which reached its maximum during the second half of the 20th century. In contrast, the precipitation anomalies are associated with the atmospheric circulation and, especially during winter, are characterized by large-scale patterns. Therefore, the anomaly field can be adequately estimated by interpolating fewer stations in a sparse station-network period (i.e. the 19th century).

The density of the station network available in the GAR, with a bicentennial time length, is among the best that can be found in global instrumental climatic records. However, the complexity of the GAR (mainly due to the presence of the Alpine mountain chain) makes it difficult to develop a domain-wide statistical model for interpolating the whole precipitation field. Instead, a local interpolation technique was applied to the time-varying station network.

The interpolation technique used is based on inverse-distance-weighted (IDW) averaging of neighboring time series of each grid cell across the GAR. A particular version of this technique is the angular-distance-weighted (ADW) interpolation, since it includes an ‘angular’ term which accounts for the geographical separation of the sites of the time series. It was originally developed by Shepard who called it the ‘Synagraphic Mapping System’ (SYMAP) algorithm [Shepard, 1968, 1984; Willmott *et al.*, 1985]. The technique relies on the fact that the inter-relation of station time series decreases with distance, both in terms of the time-mean and the variability. Thus in terms of local averaging, it is reasonable to assign higher weights to nearby-located time series than to remote ones. Moreover, since the time series averaged are, in general, unevenly distributed in space, the angular separation between the sites of the interpolated time series is taken into account by avoiding over-weighting of information from the same sector: well-separated time series are more strongly weighted than nearby ones. Therefore, the weight $w(k)$ of each time series is the outcome of a product:

$$w(k) = w_{rad}(k) w_{ang}(k) \quad (2)$$

where w_{rad} (the ‘radial term’) is a function of radial distance from the target grid-cell (see Figure 6a) and w_{ang} (the ‘angular’ or ‘directional term’) is a function of the angular separation of the sites from other interpolated time series with respect to the grid-cell combined with their radial terms:

$$w_{ang}(k) = 1 + \frac{\sum_{l=1}^n w_{rad}(l) [1 - \cos \theta_j(k, l)]}{\sum_{l=1}^n w_{rad}(l)}, \quad l \neq k \quad (3)$$

Here $\theta_j(k, l)$ is the angular separation of data stations k and l with the vertex of the angle defined at grid point j (see Figure 6b).

As mentioned previously, the augmented ETH climatology provided the time-mean field for the GAR. Since it refers to the 1971–1990 period the station time series anomalies $\psi_r(s, t)$ were also derived with regard to their 1971–1990 mean $\langle \psi(s) \rangle$. Following the methodology of the studies of *New et al.* [2000] and *Widmann and Bretherton* [2000], the anomalies $\psi_r(s, t)$ were multiplicative, i.e. they were derived as ratios:

$$\psi_r(s, t) = \frac{\psi(s, t)}{\langle \psi(s, t) \rangle} \quad (4)$$

and not additive (i.e. $\psi_d(s, t) = \psi(s, t) - \langle \psi(s) \rangle$), although the latter is the most commonly used in climatic data interpolation. There are a number of reasons for this:

a) The application of the ADW technique implies a spatially-isotropic distant-dependent inter-association of the field within the geographical domain, a condition that is frequently not satisfied due to orographic effects on precipitation which are predominant in the GAR. Mean precipitation at nearby stations within the GAR may differ by $\pm 20\%$, while in some cases exceeds $\pm 100\%$ (i.e., double precipitation, on the long-term, recorded at adjacent stations). With the variance of station time series being analogous to its time-mean precipitation, an interpolation of additive anomalies would lead to an interpolated result with variance biased in favor of the most strongly varying time series [Paulhus and Kohler, 1952]. The derivation of precipitation anomalies as ratios from the mean field results in variance-normalized time series with the resulting regression coefficients close to unity. Although the standard deviation is a more accurate normalization factor, use of the time-mean (climatology) was examined and found to be more robust when the statistics are calculated for the rather short period of 20 years.

b) Interpolation of additive anomalies may yield negative monthly precipitation totals (after the re-addition of the mean field), which results from interpolation of exceptionally low-precipitation for dry months. This side effect is avoided in interpolation of multiplicative anomalies because the potentially minimum resultant value is zero.

The radial term used to interpolate the multiplicative anomalies is shown in Figure 6a. It was defined after conducting EOF-based (see following subsection 3.1) experimental reconstructions of station time series for the 1931–2000 (HISTALP station-mode data) and 1961–2000 (MeteoSwiss data) periods. Each individual time series was reconstructed as a linear combination of weighted time series from neighboring stations. The corresponding radial term was estimated by calculating the weights for each station in relation to the distance from the station reconstructed. The final radial term was the outcome of averaging over a multitude of cases (reconstructions through various combinations of stations) and was used for all months, although its form actually varies from season to season.

The overall gridding procedure consists of four steps: a) reconstruction of incomplete station series b) derivation of the “anomaly field” with respect to the 1971–1990 station-based climatology, c) interpolation of the anomalies onto a $10\text{min} \times 10\text{min}$ grid, and d) merging of the gridded climatology (mentioned in section 2.2) and the gridded anomaly field to derive the (full) gridded field in mm units. Step (a) is described in subsection 3.1, whereas steps (b), (c), and (d) are given in subsection 3.2.

In developing the HISTALP 10-min-grid data set, apart from the Pearson correlation coefficient being used (hereafter shortly referred to as ‘correlation’), an integrated quantitative index is also employed: the ‘variance explained’ score. It is defined as:

$$\text{Variance explained} = \left(1 - \frac{\text{Variance}(P - P_{ref})}{\text{Variance}(P_{ref})} \right) \times 100 \quad (1)$$

where P_{ref} is the reference station/grid-point time series and P is a computed series. If P_{ref} is a station series, P represents the reconstructed series using nearby station data; if P_{ref} is a grid-point series calculated by interpolation from a group of nearby station data, P represents the re-computed grid-point series using a selection of data from different, more remote, stations. The variance explained score reflects the joint aspects of the correlation coefficient and the match/difference of variances of the two series compared. It is a relative measure, with respect to the characteristics of the reference series, and is expressed on a per cent scale, with 100% being the maximum value assigned to a perfect match between P_{ref} and P (both in terms of temporal variability and magnitude of variations).

3.1. Reconstruction of Incomplete Station Series

A particular problem with the monthly time series of the HISTALP station-mode data set is that the individual series have different periods of record. Their number decreases from 1926 back to 1800 (see Figure 2). Thus a straightforward interpolation of the existing station time series will lead to a spatially

smoothed gridded anomaly field, especially during the first decades of the 19th century when only a few stations provide observations. However, the HISTALP station-mode data set availability for most of the decades of the 20th century provides information on the spatio-temporal covariance of the anomaly field which can be used to reconstruct the missing values in the time series. Reconstruction of individual time series prior to gridding interpolation should moderate smoothing effects. For this purpose, linear regression with a nearby, well-correlated time series has been used in previous studies [e.g., *Widmann and Bretherton* 2000; *Gyalistras*, 2003] to fill gaps in station time series. Such a method tends to replicate information from neighboring station data; it is nevertheless effective for data gaps that a) are short in comparison with the total length of the target time series and b) do not occur simultaneously at large spatial scales (i.e. the same temporal gaps in many station time series). More accurate reconstructions have been achieved, however, through multiple regression of more than one time series [e.g., *Tabony*, 1983; *Young*, 1992; *Eischeid et al.*, 1995; *Xia et al.*, 1999; *Eischeid et al.*, 2000]. The improved reconstruction results from the suppression of the very local variability inherent in each regressed time series which increases the percentage of the large-scale precipitation signal in the reconstructed time series. A shortcoming of the above methods is that the regression coefficients tend to provide a best fit for the variability in the specific period for which they have been defined; their use for other periods implies an assumption that the precipitation field is stationary. If stationarity is less strong, then the reconstructed time series will deviate from the real climatic signal. To reduce such effects, a less strict method has been applied in this study.

The reconstruction method used is based on the use of spatial empirical orthogonal functions (EOFs; see *Jolliffe* [2002]) defined by the analysis of time series in the data-complete period, from 1931 to 2000 (70 years). The EOFs defined were projected onto the existing data of previous decades to reconstruct the missing values. Aiming to minimize the approximation error of each EOF projection, for each missing monthly value of an incomplete time series, only time series with data available at that time were considered to define the EOFs. Moreover, among the data available, only a small number of the nearest stations with significantly-correlated time series with the time series under reconstruction were selected. At least 3 time series were required to define the local EOFs (in order to guarantee a reliable and temporally stable reconstruction); the number of selected time series could increase if additional series would lead to a noticeable enhancement of the reconstruction skill. On average, 6–7 series were used for local EOF definition (up to 20 in some rare cases). An EOF was used back in time until the station network varied and then a new EOF, according to data availability, needed to be defined. Particular care was also taken for years with large outliers; they were identified through bivariate linear regressions of the selected stations against the reconstructed time series (within the 1931–2000 period). These years were not included in the definition of EOFs.

The EOF-based reconstruction was carried out for each calendar month separately, since the EOFs are not the same throughout the seasons. Instead of using a subgroup from the first EOFs (ranked according to the variance explained), the reconstruction was implemented in an iterative way: at each iteration only the first EOF was projected, the reconstructed component was then subtracted from the whole precipitation field, and the residual field was again re-analyzed. The iterative reconstruction was terminated when the residual field consisted of non-significantly correlated time series. This termination rule restricted the introduction of local-scale climate variability and non-climatic noise into the reconstructed time series. Therefore, the iterative approach enabled a monitoring of the reconstruction progression by using only statistically significant information for approximating the missing data. An evaluation of this method against the multiple regression approach indicated that, although the latter is slightly better, the two approaches have similar accuracy outside the calibration period, and, in particular, the EOF-based technique performs nearly equally well within and outside the calibration period (see Appendix A). As a consequence, the predicted reconstruction skill outside the calibration period is more reliable when EOFs are used.

The EOF-based technique developed here has common characteristics with other reconstruction/data imputation techniques used in other studies. For instance, working at a regional scale (instead of domain-wide analysis) was recommended by *Gebhardt et al.* [2000] and *Wasito and Mirkin* [2005] for complex field analysis. Moreover, iterative/convergence-oriented approaches were used by *Beckers and Rixen* [2003] and in implementations of the expectation–maximization (EM) algorithm [e.g., *Dempster et al.*, 1977; *Little and Rubin*, 1987; *Ghahramani and Jordan*, 1994]. In particular, the regularized expectation–maximization (RegEM) algorithm of *Schneider* [2001], in which regression coefficients are estimated by ridge regression, has been shown to perform better in the presence of a nonstationary behavior of the climate field, as long as an adequate EOF definition period is used [*Rutherford et al.*, 2003].

The application of the EOF technique to a station network, with declining data back in time and with the distance of the selected stations varying throughout the reconstruction period, resulted in reconstructed time series whose skill (i.e., explained variance, estimated within the EOF-definition period) also varied. Larger inter-station distances and lower skill are found in the early 19th century. June and July are the months with the poorest reconstruction results, both in terms of the number of reconstructed years and reconstruction skill scores (Figure 7a). This is a consequence of the less coherent precipitation field during summer months where convective processes dominate, in contrast to winter months where large-scale atmospheric circulation–related precipitation patterns dominate. However, the reconstruction skill varies across the GAR. In particular, inferior skill scores are found across the Alps in comparison to the surrounding plains (Figure 7b). In parts of Croatia and Bosnia–Herzegovina, especially low skill scores are observed in April (Figure 7c). The number of time series reconstructed using the EOF method is given by the histogram of Figure 7d.

3.2. Data Interpolation

With the individual station time series reconstructed, an ADW interpolation was then carried out. The interpolation was applied to multiplicative station time series anomalies with regard to their 1971–1990 mean. For each grid cell, the 3 nearest station time series (either with observed or reconstructed values) were used in the interpolation. Distance from the grid cell was not the only criterion in selecting the time series; another condition was set to account for the case of adjacent climatic zones with sharp transitions between them. Such a case exists in winter between the northern and southern side of the Alpine mountain chain. To avoid interpolating times series from different climatic zones, the selected time series should be significantly correlated with the station time series nearest to the grid cell. Significance levels were determined by the typical correlations found between neighboring time series for each particular calendar month. For the early years of the 19th century where only a few station time series are available, the predefined significance levels were gradually relaxed down to the 95% significance level until the requirement for 3 station time series was satisfied. No interpolation was attempted if this condition (3 correlated series) was not met.

The interpolation onto the 10min × 10min grid yielded the anomaly field with respect to the 1971–1990 mean. The full field, in mm units, was calculated after multiplying the interpolated field with the augmented ETH climatology data set.

3.3. Interpolated Field Accuracy

Along with the monthly precipitation interpolation at grid points, the relative explained variance score, with respect to the 1931–2000 precipitation field (which is within the 1927–2003 period, with full availability of station network observations), was also calculated. The scores were estimated by applying the same weights used for the reconstruction and interpolation throughout the 19th to 20th Centuries to the time series during the 1931–2000 reference period and then comparing the outcome with the original 1931–2000 interpolated time series. The explained variance score is a nearly monotonically increasing function with time from 1800 to 1927 for each individual calendar month. From 1927 to 2003 the score is 100%, for all months, with an exception for January 2003 due to a missing station datum. Since the

explained variance score depends on the skill of station-based time series (either observational or reconstructed) being interpolated, the geographical characteristics and the intra-annual variation of the station and grid time series scores are closely inter-associated. Hence, higher grid scores are found in winter months, whereas the lowest scores characterize the June and July time series (Figures 8a and 8b). In particular regions (e.g., mountains, the southeast GAR), the grid scores are locally low (Figures 8b and 8c).

The time evolution of the explained variance score sometimes exhibits a strange behavior: the sparseness of observational data in the first decade of the 19th century has led to some anomalous scores there. Also there are a few drops of score afterwards, most of them less than 5% (Figures 8a–8c). These phenomena result from the gridding method (both at reconstruction and interpolation stages) which gives some preference to the selection of the nearest available data. Hence, as the data-providing station network gets denser through the course of years, some nearby data selected, either for station time series reconstruction or grid-point time series construction, come from station time series which may be less correlated with the station/grid-point time series under construction in the reference period (i.e. from 1931 to 2000) than some more distant time series. Therefore, the resultant reconstruction / interpolation may have lower scores than if distant data were used. In some cases there is a clear physical reason for the higher correlation of distant time series than the nearby ones: e.g. precipitation field partitioning into zones due to the presence of mountain chains. Particular adaptations have been applied to the data analysis method to take into account such cases, which led to re-computation of several station-series reconstructions and re-derivation of grid-point series: data from a wider group of stations were selected, wherever that selection resulted in a significant increase of the explained variance score. However, the adaptations did not aim to eliminate every anomalous score evolution, since the score is estimated within a specific reference period (1931–2000) which may not be representative of the exact precipitation field structure in previous decades. By assuming that the precipitation field is to some extent non-stationary, we preferred to select nearby data, even if they were from less-correlated time series (provided that the correlation difference was not large), since distant correlations are, in general, less stable in time.

Not all the gridded precipitation data during the 19th & 20th Centuries are usable: a realistic gridded precipitation time series should have positive explained variance scores. Moreover, a meaningful gridded field appears to correspond to scores of at least 60%. The number of gridded precipitation time series, with year-round monthly scores above that level, is shown in Figure 8d.

4. Evaluation of the Gridded Precipitation Data Set

A preliminary evaluation has been conducted to identify similarities and discrepancies between the new HISTALP 10-min-grid data set and some of the station-based and grid-based data sets. The evaluation of the gridded precipitation data set has focused on two aspects: a) the inter-consistency against the station time series used for the data set development, and b) the comparison with the independently developed CRU ($0.5^\circ \times 0.5^\circ$), ETH ($0.30^\circ \times 0.22^\circ$), and CHCAM ($0.05^\circ \times 0.05^\circ$) data sets. Station data from regional meteorological networks were also considered. The parameters examined were the correlation of interannual variability, multidecadal trends and spatial correlation of extreme precipitation patterns.

4.1. Correlation Analysis

4.1.1. HISTALP 10-min-grid vs HISTALP station-mode

Firstly, the time series of each HISTALP station time series were compared with the nearest grid-point time series. The correlation between the two data sets during the 19th and 20th Centuries is very high (see Figure 9 for the 1931–2000 period). The lowest correlations are found in summer months. Low correlations are also found for some station sites in mountainous regions. Also, the spatial patterns of

anomalies (expressed in per cent deviation from the 20th century mean) of the station and grid-point data match each other well (Figures 10a and 10b). The reliability of the anomalies has been evaluated through the relative explained variance score, both for station and grid-point time series. Similar spatial patterns of the score for the station network and the grid are observed for the individual monthly maps (Figures 10c and 10d).

4.1.2. HISTALP 10-min-grid vs Other Data Sets

When gridded field data sets were compared, spatial sub-sampling was applied to the comparatively higher-resolution data set, prior to correlation analysis, in order to compare the data sets on a common grid. Thus, the HISTALP 10-min-grid field was sub-sampled, when compared with the slightly coarser ETH and much coarser CRU fields, whereas when compared with the CHCAM field, the latter data set was spatially averaged onto the 10min × 10min grid.

A good match with the ETH data set was found for the 1901–1990 period. Higher correlations are observed in winter months, but with some low correlations, mainly along the main Alpine mountain chain and also over the eastern part of Massif Central (Figure 11a). In summer, correlations are lower, particularly in southeast France and along the Ligurian Sea coastline (Figure 11b), where the station networks used for developing the two data sets are quite different (see Figure 4a).

Furthermore, significant cross-correlations with the CRU data set were found, mainly in the northern parts of the GAR (Figures 11c and 11d). However, the correlations are not as high as those found with the ETH data set. The high/low correlation contrast, between winter and summer months, is again observed. The main Alpine mountain chain, northwest Austria and south of 44°N in the Italian Peninsula are the regions with the lowest correlations. Note that the correlations reported here refer to the 1901–1990 period, during which the CRU station network varied. In the early decades of the 20th century, when less data were used for developing the CRU data set, the HISTALP 10-min-grid – CRU correlations exhibit further reduced values in northeast Italy and northwest Austria.

Finally, the comparison with the CHCAM data set within the Swiss territory showed that the two data sets provide fields with similar variability (Figure 12). Discrepancies are found in mountainous parts of southern Switzerland where the station networks used are both sparse and the precipitation field is less coherent. The discrepancies are larger in summer. Especially, at the high-altitude grid-cells around ~ 8°E and 46.5°N, the two data sets exhibit very low correlations in non-winter months (April–October). These grid-cells do not include stations from either of the station networks used for developing the two gridded precipitation data sets and hence the estimated field is a result of interpolation from out-of-the-grid-cell station data in both data sets.

4.2. Multidecadal Trends

Multidecadal trends computed from all the long-term data sets were compared. January and October were selected since the strongest 20th century trends are exhibited during these months. The station and grid-point data provided similar patterns, although the gridded field appears to have ~5% reduced trends (mainly for the strongest trends) compared to the station data. Regarding the independent data sets, the ETH-estimated trends match better the trend patterns of the HISTALP 10-min-grid field than the CRU-estimated trends, although the latter exhibit good agreement in the eastern GAR, where ETH data were not available (Figure 13). Over the 19th century only HISTALP station-mode and HISTALP 10-min-grid fields were compared. Both fields demonstrate that there are some contrasting patterns of opposite trends on different sides of the main Alpine chain (not shown).

In Switzerland the CHCAM data set provides a detailed picture of the local trends. The HISTALP 10-min-grid data set provides roughly similar trend patterns (Figure 14). The match between the trend patterns of the two data sets is better for the lower-altitude and denser-observed northwestern part of Switzerland. Over the Alpine mountain chain the match is poorer. Note that, as mentioned above, the Alpine divide appears to delimit different trend patterns in some winter months.

4.3. Cases of Excessive Precipitation

One of the potential risks of the methods used to merge a spatially highly resolved shorter climatology with long-term spatially scarcer interpolated fields is an exaggeration of single events of excessive precipitation which may not follow the usual patterns derived from the mean climatology. A respective bias of the gridded fields would degrade the value of the data set for extreme event analyses – a topic of great importance in recent climate studies. We therefore extracted all of the most extreme cases in the gridded fields and analysed them for a potential bias. The chosen threshold was a monthly precipitation total of 800mm, which is very near to the measured maximum values in the HISTALP station series (which are between 800 and 810 mm). Thirty-one such excessive precipitation events could be found in the gridded data set and were cross-checked against additional station data from hydrological and meteorological yearbooks.

Two cases of excessive precipitation are presented here, at times where that station network is not sparse, i.e., for October 1889 and November 2002. For the October 1889 case, affecting Italy, Austria and Slovenia (Figure 15a), the gridded precipitation is compared against the HISTALP station-mode data enriched with additional local station data. For the November 2002 case, occurring in the Swiss Ticino and Italian Piedmont and Lombardy regions (Figure 15b), the gridded precipitation is compared against independent MeteoSwiss station data and regional station network data from Italy. In both cases the correlation between the compared data is good despite, some scattering from the 1:1 line (Figures 15c and 15d). To examine the influence of spatial coherence of the station data on the gridded–station data deviations, each station datum was compared with neighboring station data. If at least three stations within 20km radius were found, the median value of that group was compared with the station datum under investigation. The examination demonstrated that the strongest gridded–station data deviations correspond to station data identified as ‘outliers’ (see Figures 15c and 15d).

4.4. Remaining Uncertainties

Since the HISTALP 10-min-grid data set relies on the data sets used for its development, any inaccuracy of the augmented ETH climatology and the HISTALP station-mode data set (either sporadic or systematic) will also be transferred to the new data set. The potential user should, therefore, should be aware that:

- a) The intra-annual variability of certain areas of the GAR (most possibly in the far-east and southeast) may not be so accurate due to the sparse station network used for developing the local climatology there, as was noticed in section 2.3. Other effects may also be important. For example, systematic measurement errors, such as precipitation undercatch due to the influence of wind and type of precipitation, need to be quantified too. In Appendix B, a preliminary assessment of climatology-related uncertainties is briefly presented.
- b) Although extensive homogenization has been applied to the original HISTALP station data, there may be effects that could have introduced non-negligible errors to the homogenized HISTALP station-mode data set. As mentioned above, the effects of wind and solid precipitation (especially during winter) may have led to undercatch of the total precipitation that fell at the station sites. The comparison of the (uncorrected) HISTALP 10-min-grid 1961–1990 averages with the (corrected) ÖKLIM 1961–1990 climatology (see Appendix B) illustrates the magnitude of the uncertainty. Although snow undercatch has been shown to have only marginal effects on long-term trends [Schmidli *et al.*, 2002], a thorough study is needed to shed further light onto the various aspects of temperature and wind impacts on the measured precipitation.
- c) High Alpine sites (>1500m above sea level) are not well covered by the HISTALP stations, despite the virtually even distribution of the station network across the GAR (see Figure 1). The highest stations are at altitudes of 1600 to 1900m and are located at high-elevation valley sites, not summit sites [Auer *et al.*, 2005]. There are 4 stations at an altitude > 1500m, but none of them provides any record before 1860 (see Figure 2e). Apart from the precipitation measurement problems at high altitudes (due to solid

precipitation), the precipitation field is markedly less coherent over the Alps, a fact reflected by the low explained-variance scores estimated for the 19th century gridded precipitation (Figure 10). Therefore, high-alpine precipitation is relatively poorly represented by the HISTALP 10-min-grid data set.

d) Although the HISTALP 10-min-grid data set was constructed from homogeneous station records, the variations in the density of the station network can result in inhomogeneities in the gridded analysis. For example, the interpolation from more remote stations with the coarser network in earlier periods is expected to have a stronger smoothing effect and hence give a smaller variance than during periods with denser networks. Such inhomogeneities are particularly relevant for the study of extremes, because extremes are very sensitive to changes in variance [e.g., *Katz and Brown*, 1992]. Therefore, care should be exercised in the comparison of extremes between periods with variable networks and, in particular, in trend analyses. The reliability of results from the gridded analysis should be compared with those from the available station data.

The identification of the relative importance of the effects mentioned above and the application of appropriate adjustments together with inclusion of additional data could lead to further improvement of the derived HISTALP 10-min-grid data set, but this is left for future studies.

5. Conclusions

The construction of the new HISTALP 10-min-grid data set aims to represent the precipitation variability over the Greater Alpine Region on a regular geographical grid with monthly time resolution. To cope with the complexity of the precipitation field in the GAR a local data interpolation technique was developed which was applied to the time-varying station network. The parameters of the local interpolator were determined by the precipitation field coherence and the data availability around each grid cell. The gridding was implemented in two stages: a) reconstruction of the individual station time series using neighboring station data, and b) angular-distance-weighted (ADW) interpolation of observational and reconstructed monthly data. The temporal evolution of the gridded precipitation field accuracy was estimated in relation to the full station network period (1931–2000). The relative explained variance (score) computed indicates that the accuracy declines back in time as the station network becomes sparser, particularly in the inner-Alpine region during the 19th century. The accuracy also varies throughout the calendar year, with comparatively lower scores during the summer, due to reduced spatial coherence of rainfall patterns at that time. Within the 20th century, the gridded field compares well with the field provided by other data sets, in terms of the temporal variability correlation and multidecadal trends. Discrepancies were also found locally, mainly at places and times where the station networks of the various data sets differ substantially. While the new data set surpasses other gridded precipitation data sets, in terms of time length, its reliability has to be further validated through its use in future climate studies.

Appendix A

Use of EOFs for reconstruction tacitly implies that they are stationary: the EOFs identified in the calibration period (i.e. the EOF-definition period) are similar with the EOFs that could be derived in the reconstruction period, if the missing data were known. In addition, the calculated variance explained score for the quality of the reconstructed and gridded precipitation assumes that the EOFs used are stable in time. To examine the stability of EOFs used and the reliability of the reconstruction skill used in this study, we have performed a comparison of the reconstructed time series period against observations outside the calibration period, i.e. from 1861 to 1930. Thus only series with complete observations from 1861 and onwards were used in these experimental reconstructions (63 in total). Six stations close to each

reconstructed station were selected to simulate the average number of stations used in the overall reconstruction of GAR precipitation. The reconstruction skill was then computed for each station (a) within the calibration period, and (b) within the reconstruction period. Since the reconstruction skill depends on the correlations with the EOF-analyzed time series, the skill was averaged according to the maximum correlation within the group of the stations selected. Results are shown in Figure A1a, where, for comparison, statistics from the use of multiple regression is also shown. The two techniques produce similar results, with the regression being slightly better within the calibration period, with the EOF-based reconstruction performing similarly within and outside the calibration period. The reason for finally selecting the EOF-based technique for reconstructing the GAR precipitation is that it is more robust in time by avoiding the overfitting that can occur with multiple regression in respect of the calibration period variability. It should be noted that this advantage of the EOF-based technique (as developed in our study) is even more pronounced when the calibration period is short (e.g., for 20 years; see Figure A1b), although this is not the case in our study.

Appendix B

The HISTALP station-mode and ETH climatology data sets were used without further data homogenization; the climatology was only geographically augmented to cover the whole GAR. Although the objective of this study is focused on the development of a gridded precipitation data set (constrained by the availability and accuracy of the data used), we have attempted to compare the potential effects of using two alternative climatologies at national scales, for Austria and Slovenia, which are based on station networks that are locally denser than that of the augmented ETH climatology. The characteristics of these two regional climatologies are described below together with a brief comparison with the climatology of the HISTALP 10-min-grid data set.

B1. ÖKLIM Climatology (1961–1990)

Auer et al. [2001b] developed Oct–Mar, Apr–Sep and Jan–Dec seasonal precipitation climatologies at $250 \times 250\text{m}$ resolution for Austria based on nearly the same station network as the Austrian part of the ETH climatology (1971–1990) but undertaken with another interpolation procedure and based on a different time period. 954 single measuring sites with mainly daily readings in the recent World Meteorological Organization (WMO) “CLINO period” (1961–1990) were used. Some of these (the less accessible storage gauges in high-elevation regions) had monthly to (in single cases only) annual readings. In contrast to the ETH climatology, a procedure was applied in ÖKLIM to correct for systematic measurement errors (influence of wind, type of precipitation; see *Ungersböck et al.* [2001] for details). To achieve statistically significant regressions between precipitation measurements and elevation, interpolation was done for seasonal periods Oct–Mar, Apr–Sep only. The interpolation is based on a twofold procedure: in a first step the vertical structure of precipitation (deterministic part) is eliminated by regionalized regressions and in a second step remaining residuals (stochastic part) are interpolated by means of a kriging approach. Large-scale regressions (like lat–long dependencies, ocean–continent gradients for example) were also tested but turned out to be strongly outweighed by the orographic effects of the Alps [*Auer et al.*, 2001c].

The ÖKLIM climatology was compared with the HISTALP 10-min-grid climatology for the 1961–1990 period. Half-year averages were compared: one for the winter half of the calendar year (October to March) and a second one for the summer half (April to September). The difference between the two climatologies is illustrated in Figures B1a and B1b. There is higher precipitation in the winter ÖKLIM climatology across Austria with larger differences over the mountainous part of the country. In summer, the differences are sporadic and do not constitute coherent patterns.

B2. Slovenian Climatology (1961–1990)

In the year 2000, the Climatology Department of EARS (Environmental Agency of the Republic of Slovenia) developed monthly gridded climatologies (1961–1990) for precipitation (unpublished data, provided by M. Dolina, 2005) as an addendum to the ‘Climatography of Slovenia’. The final resolution of the precipitation maps is 100×100 m. The value of precipitation at every grid point was calculated using a residual kriging model. In the deterministic part of the model the relationships between the monthly precipitation climatology and geographical variables (altitude, latitude and longitude) were considered. The biases of the deterministic part of the model were interpolated using a spherical variogram model with various sills and ranges for different months, while the radius of influence was kept constant (35 km) for all 12 months. In addition to monthly station data from the ‘Climatography of Slovenia’ [Zupancic, 1995], corrected measurements from totalizers in mountainous terrain were used too. For spatial interpolation only data from Slovenian measurement networks were used. This is the reason for larger uncertainties associated with precipitation values on the mountainous border with Italy and Austria. Larger uncertainties are also possible in regions of very high precipitation gradients (e.g. Trnovski gozd, Snežnik), where the measurement network is too sparse to measure precipitation accurately.

As for the ÖKLIM climatology, winter and summer half-year averages of the Slovenia climatology were compared with the HISTALP 10-min-grid climatology for the 1961–1990 period. The comparison outcome is given in Figures B1c and B1d. It is apparent that, apart from some noticeable differences found over the mountainous parts of the country (in the South and West), the two climatologies are quite similar (differences within $\pm 10\%$).

It is to be expected that the largest differences found here (especially the Austrian winter ones) are primarily due to the corrections of measurement biases. Whether or not these correction procedures indeed provide a more realistic analysis of the precipitation climate is however unclear. For example, bias correction in Switzerland led to a more consistent water-balance in some river catchments, but it resulted in large inconsistencies for many others especially at higher altitudes [Schädler and Weingartner, 2002]. Thus further analyses are required to reduce the uncertainties of the precipitation climatology of the GAR.

Acknowledgements. This study was carried out in the framework of the ALP-IMP project supported by the European Commission (EVK2-CT-2002-00148). The HISTALP system was developed within the Austrian Science Fund (FWF)–funded project CLIVALP (P15076-N06). We thank both anonymous reviewers for their extensive and helpful reviews. We would also like to thank all the ancillary precipitation data providers which made possible the evaluation of the HISTALP 10-min-grid data set: Michael Begert for the MeteoSwiss station data, Dimitrios Gyalistras for the Swiss climatology and anomaly data sets, Mojca Dolina for the Slovenia climatology, Daniele Cat Berro for the Piedmont region station data, and Angela Sulis for the Lombardy region station data.

References

- Auer, I. (1993), Niederschlagsschwankungen in Österreich (Precipitation variability in Austria), *Österreichische Beiträge zu Meteorologie und Geophysik*, 7, 1–73.
- Auer, I., and R. Böhm (1994), Combined temperature-precipitation variations in Austria during the instrumental period, *Theor. Appl. Climatol.*, 49(3), 161–174.
- Auer, I., R. Böhm, and W. Schöner (2001a), Austrian long-term climate 1767–2000, multiple climate time series from Central Europe, *Österreichische Beiträge zu Meteorologie und Geophysik*, 25, 1–147.
- Auer, I., R. Böhm, H. Mohnl, R. Potzmann, W. Schöner, and P. Skomorowski (2001b), *ÖKLIM–Digitaler Klimaatlas Österreichs* (ÖKLIM – digital climate atlas of Austria) [CD-ROM], Central Institute for Meteorology and Geodynamics (ZAMG), Vienna, Austria.
- Auer, I., R. Böhm, H. Mohnl, R. Potzmann, W. Schöner, and P. Skomorowski (2001c), *ÖKLIM – Der digitale Klimaatlas Österreichs*, *Österreichische Beiträge zu Meteorologie und Geophysik*, 27, DACH 2001 [CD-ROM] , Central Institute for Meteorology and Geodynamics (ZAMG), Vienna, Austria.
- Auer, I., et al. (2005), A new instrumental precipitation dataset for the Greater Alpine Region for the period 1800–2002, *Int. J. Climatol.*, 25(2), 139–166.
- Beck, C., J. Grieser, and B. Rudolf (2005), A new monthly precipitation climatology for the global land areas for the period 1951 to 2000, in *Climate Status Report 2004*, German Weather Service, Offenbach, Germany.
- Beckers, J., and M. Rixen (2003), EOF calculations and data filling from incomplete oceanographic datasets, *J. Atmos. Oceanic Technol.*, 20(12), 1839–1856.
- Böhm, R. (1992), Lufttemperaturschwankungen in Österreich seit 1775 (Air temperature variability in Austria since 1775), *Österreichische Beiträge zu Meteorologie und Geophysik*, 5, 1–95.
- Daly, C., R. P. Neilson, and D. L. Phillips (1994), A statistical-topographic model for mapping climatological precipitation over mountainous terrain, *J. Appl. Meteorol.*, 33(2), 140–158.
- Daly, C., W. P. Gibson, G. H. Taylor, G. L. Johnson and P. Pasteris (2002), A knowledge-based approach to the statistical mapping of climate, *Clim. Res.*, 22(2), 99–113.
- Dempster, A. P., N. M. Laird, and D. B. Rubin (1977), Maximum likelihood from incomplete data via the EM algorithm, *Journal of the Royal Statistical Society, Series B*, 39(1), 1–38.
- Eischeid, J. K., C. B. Baker, T. R. Karl, and H. F. Diaz (1995), The quality control of long-term climatological data using objective data analysis, *J. Appl. Meteorol.*, 34(12), 2787–2795.
- Eischeid, J. K., P. A. Pasteris, H. F. Diaz, M. S. Plantico, and N. J. Lott (2000), Creating a serially complete, national daily time series of temperature and precipitation for the western United States, *J. Appl. Meteorol.*, 39(9), 1580–1591.
- Frei, C., and C. Schär (1998), A precipitation climatology of the Alps from high-resolution rain-gauge observations, *Int. J. Climatol.*, 18(8), 873–900.
- Gajic-Capka, M., M. Percec Tadic, and M. Patarcic (2003), Digitalna godisnja oborinska karta Hrvatske (A digital annual precipitation map of Croatia), *Hrvatski Meteoroloski Casopis (Croatian Meteorological Journal)*, 38, 21–33.
- Gebhardt, C., B. Kusserow, and A. Hense (2000), Optimal averaging of incomplete climatological data, *Theor. Appl. Climatol.*, 65(3–4), 137–155.
- Ghahramani, Z., and M. I. Jordan (1994), Supervised learning from incomplete data via an EM approach. Advances, in *Advances in Neural Information Processing Systems 6*, edited by J. D. Cowan, G. Tesauro, and J. Alspector, pp. 120–127, Morgan Kaufmann, San Francisco, CA.
- Gyalistras, D. (2003), Development and validation of a high-resolution monthly gridded temperature and precipitation data set for Switzerland (1951–2000), *Clim. Res.*, 25(1), 55–83.

- Huffman, G. J., R. F. Adler, M. M. Morrissey, D. T. Bolvin, S. Curtis, R. Joyce, B. McGavock, and J. Susskind (2001), Global precipitation at one-degree daily resolution from multi-satellite observations, *Journal of Hydrometeorology*, 2(1), 36–50.
- Hutchinson, M. F. (1995), Interpolating mean precipitation using thin plate smoothing splines, *Int. J. Geogr. Inf. Syst.*, 9(4), 385–403.
- Hutchinson, M. F. (2000), ANUSPLIN version 4.1 user guide, 51 pp., Centre for Resources and Environmental Studies, Australian National University, Canberra, Australia.
- Jolliffe, I. T. (2002), *Principal Component Analysis*, 2nd ed., 487 pp., Springer-Verlag, New York.
- Jones, P. D., and M. Hulme (1996), Calculating regional climatic time series for temperature and precipitation: Methods and illustrations, *Int. J. Climatol.*, 16(4), 361–377.
- Jones, P. D., T. M. L. Wigley, P. M. Kelly (1982), Variations in surface air temperatures, Part 1. Northern Hemisphere, 1881–1980, *Mon. Weather Rev.*, 110(2), 59–70.
- Katz, R. W. and B. G. Brown (1992), Extreme events in a changing climate: Variability is more important than averages, *Clim. Change*, 21(3), 289–302.
- Kirchhofer, W., B. Sevruck (1992), Mittlere jährliche korrigierte Niederschlagshöhen 1951–1980 (Corrected mean annual precipitation totals 1951–1980), in *Hydrological Atlas of Switzerland. Landeshydrologie und Geologie*, edited by M. Spreafico, R. Weingartner, and C. Leibundgut, Plate 22, Institute of Geography of Bern University, Bern, Switzerland.
- Leemans, R., and W. P. Cramer (1991), The IIASA database for mean monthly values of temperature, precipitation and cloudiness of a global terrestrial grid, *Report No. RR-91-018*, International Institute for Applied Systems Analysis (IIASA), Laxenburg, Austria.
- Legates, D. R., and C. J. Willmott (1990), Mean seasonal and spatial variability in gauge-corrected, global precipitation, *Int. J. Climatol.*, 10(2), 111–127.
- Little, R. J. A., and D. B. Rubin (1987), *Statistical analysis with missing data*, John Wiley and Sons, New York.
- Menzel, L. (1999), Flächenhafte Modellierung der Evapotranspiration mit TRAIN (Spatial modeling of evapo-transpiration using TRAIN), *PIK Report No. 64*, Potsdam Institute for Climate Impact Research, Potsdam, Germany.
- Menzel, L., H. Lang, M. Rohmann (1999), Mittlere jährliche aktuelle Verdunstungshöhen 1973–1992 (Recent mean annual evaporation 1973–1992), in *Hydrological Atlas of Switzerland. Landeshydrologie und Geologie*, edited by M. Spreafico, R. Weingartner, and C. Leibundgut, Plate 41, Institute of Geography of Bern University, Bern, Switzerland.
- Mitchell, T. D., T. R. Carter, P. D. Jones, M. Hulme, and M. New (2004), A comprehensive set of high-resolution grids of monthly climate for Europe and the globe, the observed record (1901–2000) and 16 scenarios (2001–2100), *Tyndall Centre Working Paper 55*, 30 pp., Tyndall Centre for Climate Change Research, Norwich, UK.
- Neidhöfer, F. (2000), Interpolation and downscaling of precipitation in the Alps, PhD thesis, Institute of Geography of Bern University, Bern, Switzerland.
- New, M., M. Hume, and P. Jones (1999), Representing twentieth century space–time climate variability. Part I, Development of a 1961–90 mean monthly terrestrial climatology, *J. Clim.*, 12(3), 829–856.
- New, M., M. Hume, and P. Jones (2000), Representing twentieth century space–time climate variability. Part II: Development of 1901–96 monthly grids of terrestrial surface, *J. Clim.*, 13(13), 2217–2238.
- New, M., D. Lister, M. Hulme, and I. Makin (2002), A high-resolution data set of surface climate over global land areas, *Clim. Res.*, 21(1), 1–25.
- Paulhus, J. L. H., and M. A. Kohler (1952), Interpolation of missing precipitation records, *Mon. Weather Rev.*, 80(8), 129–133.
- Piper, S. C., and E. F. Stewart (1996), A gridded global data set of daily temperature and precipitation for terrestrial biosphere modeling, *Global Biogeochem. Cycles*, 10(4), 757–782.

- Rutherford, S., M. E. Mann, T. L. Delworth, and R. Stouffer (2003), Climate field reconstruction under stationary and nonstationary forcing, *J. Clim.*, 16(3), 462–479.
- Schädler, B., and R. Weingartner (2002), Ein detaillierter hydrologischer Blick auf die Wasserressourcen der Schweiz: Niederschlagskartierung im Gebirge als Herausforderung (A detailed hydrological view on Swiss water resources: The challenge of mapping precipitation in mountains), *Wasser Energie Luft*, 94(7–8), 189–197.
- Schmidli, J., C. Frei, and C. Schär (2001), Reconstruction of mesoscale precipitation fields from sparse observations in complex terrain, *J. Clim.*, 14(15), 3289–3306.
- Schmidli, J., C. Schmutz, C. Frei, H. Wanner, and C. Schär (2002), Mesoscale precipitation variability in the region of the European Alps during the 20th century, *Int. J. Climatol.*, 22(9), 1049–1074.
- Schneider, T. (2001), Analysis of incomplete climate data: Estimation of mean values and covariance matrices and imputation of missing values, *J. Clim.*, 14(5), 853–871.
- Schöner, W. (2004), The 2004-08 release of the HISTALP precipitation data set in grid mode 1, Internal project working paper of EC-project ALP-IMP, Central Institute for Meteorology and Geodynamics (ZAMG), Vienna, Austria [Available on demand via the project website <http://www.zamg.ac.at/ALP-IMP/>].
- Schwarb, M. (2000), The Alpine precipitation climate. Evaluation of a high-resolution analysis scheme using comprehensive rain-gauge data, PhD thesis No. 13911, 131 pp., Swiss Federal Institute of Technology (ETH), Zurich, Switzerland.
- Schwarb, M., C. Daly, C. Frei, and C. Schär (2001), Mean annual and seasonal precipitation throughout the European Alps 1971–1990, in *Hydrological Atlas of Switzerland. Landeshydrologie und Geologie*, edited by M. Spreafico, R. Weingartner, and C. Leibundgut, Plates 2.6 and 2.7, Institute of Geography of Bern University, Bern, Switzerland.
- Shepard, D. (1968), A two-dimensional interpolation function for irregularly-spaced data, *Proceedings of the 23rd National Conference of the Association for Computing Machinery*, ACM publication P-68, pp. 517–524, Brandon/System Press, Inc., Princeton, New Jersey.
- Shepard, D. (1984), Computer mapping: The SYMAP interpolation algorithm, in *Spatial Statistics and Models*, edited by G. L. Gaile and C. J. Willmott, pp. 133–145, D. Reidel Publishing Co., Dordrecht, The Netherlands.
- Tabony, R. C. (1983), The estimation of missing climatological data, *J. Climatol.*, 3(3), 297–314.
- Ungersböck M., I. Auer., F. Rubel, W. Schöner, and P. Skomorowski (2001), Zur Korrektur des systematischen Fehlers der Niederschlagsmessung – Anwendung des Verfahrens für ÖKLIM Karten (On the correction of the systematic error of precipitation measurement – Application of the procedure for ÖKLIM-precipitation maps), *Österreichische Beiträge zu Meteorologie und Geophysik*, 27, DACH 2001 [CD-ROM], Central Institute for Meteorology and Geodynamics (ZAMG), Vienna, Austria.
- Vose, R. S., R. L. Schmoyer, P. M. Steurer, T. C. Peterson, R. Heim, T. R. Karl, and J. Eischeid (1992), The Global Historical Climatology Network: Long-term monthly temperature, precipitation, sea level pressure, and station pressure data, Tech Rep. ORNL/CDIAC-53, NDP-041, 315 pp., Carbon Dioxide Information Analysis Center, Oak Ridge National Laboratory, Oak Ridge, Tennessee.
- Wahba, G. (1979), How to smooth curves and surfaces with splines and cross-validation, *Proceedings of the 24th Conference on the Design of Experiments*, pp. 167–192, US Army Research Office, Research Triangle Park, North Carolina.
- Wasito, I., and B. Mirkin (2005), Nearest neighbour approach in the least-squares data imputation algorithms, *Information Sciences*, 169(1–2), 1–25.
- Widmann, M., and C. S. Bretherton (2000), Validation of mesoscale precipitation in the NCEP reanalysis using a new gridcell dataset for the Northwestern United States, *J. Climate*, 13(11), 1936–1950.
- Willmott, C. J., and K. Matsuura (2001), Terrestrial air temperature and precipitation: Monthly and annual time series (1950–1999) Version 1.02, Center for Climatic Research, Department of

Geography, University of Delaware, Newark, DE [Available online at <http://climate.geog.udel.edu/~climate/>].

- Willmott, C. J., C. M. Rowe, and W. D. Philpot (1985), Small-scale climate maps: A sensitivity analysis of some common assumptions associated with grid-point interpolation and contouring, *Am. Cartogr.*, 12(1), 5–16.
- Xia, Y., P. Fabian, A. Stohl, and M. Winterhalter (1999), Forest climatology: estimation of missing values for Bavaria, Germany, *Agric. For. Meteorol.*, 96(1–3), 131–144.
- Young, K. C. (1992), A three-way model for interpolating for monthly precipitation values, *Mon. Weather Rev.*, 120(11), 2561–2569.
- Zierl, B. (2000), WAWAHAMO—a hydrological model to simulate drought in forested ecosystems, PhD thesis No. 1320, University of Freiburg and Swiss Federal Institute for Forest, Snow and Landscape Research (WSL), Birmensdorf, Switzerland.
- Zierl, B. (2001), A water balance model to simulate drought in forested ecosystems and its application on the entire forested area of Switzerland, *J. Hydrol.*, 242(1–2), 115–136.
- Zupancic, B. (1995), Klimatografija Slovenije 1961–1990, Padavine (Climatology of Slovenia 1961–1990, Precipitation), *Hydrometeoroloski Zavod Republike Slovenije*, 1–366.

Table 1. Overview of studies which resulted in gridded precipitation data sets covering the entire, or part of the GAR. Only studies with grid resolution $1^\circ \times 1^\circ$, or finer are presented. Country code names are: AT for Austria, BA for Bosnia-Herzegovina, CH for Switzerland, DE for Germany, FR for France, HR for Croatia, IT for Italy, and SI for Slovenia. Climatologies refer to monthly long-term time-means, unless differently stated.

No	Reference	Spatial Extent	Grid Resolution	Temporal Extent	Temporal Resolution
1.	<i>Legates and Willmott</i> [1990]	Global	$1.0^\circ \times 1.0^\circ$ (77 km \times 111 km)	1920–1980 (mainly)	Climatology
2.	<i>Leemans and Cramer</i> [1991]	Global	$0.5^\circ \times 0.5^\circ$ (39 km \times 56 km)	1930–1960	Climatology
3.	<i>Kirchhofer and Sevruck</i> [1992]	CH	1 km \times 1 km	1951–1980	Climatology
4.	<i>Auer</i> [1993]	AT	$1.0^\circ \times 1.0^\circ$ (77 km \times 111 km)	1845–1990	Monthly
5.	<i>Zupancic</i> [1995]	SI	100 m \times 100 m	1961–1990	Climatology
6.	<i>Piper and Stewart</i> [1996]	Global	$1.0^\circ \times 1.0^\circ$ (77 km \times 111 km)	1987	Daily
7.	<i>Frei and Schär</i> [1998]	AT, BA, CH, DE, FR, HR, IT, SI	$0.30^\circ \times 0.22^\circ$ (25 km \times 25 km)	1971–1990	Daily & Climatology
8.	<i>Menzel</i> [1999] <i>Menzel et al.</i> [1999]	CH	1 km \times 1 km	1973–1992	Climatology
9.	<i>New et al.</i> [1999]	Global	$0.5^\circ \times 0.5^\circ$ (39 km \times 56 km)	1961–1990	Climatology
10.	<i>Neidhöfer</i> [2000]	CH	30" \times 30" (640 m \times 920 m)	1961–1994	Climatology (seasonal & annual)
11.	<i>New et al.</i> [2000]	Global	$0.5^\circ \times 0.5^\circ$ (39 km \times 56 km)	1901–1998 (updated)	Monthly
12.	<i>Huffman et al.</i> [2001]	Global	$1.0^\circ \times 1.0^\circ$ (77 km \times 111 km)	1997–present	Daily
13.	<i>Auer et al.</i> [2001]	AT	250 m \times 250 m	1961–1990	Climatology (6-month)
14.	<i>Schmidli et al.</i> [2001, 2002]	AT, BA, CH, DE, FR, HR, IT, SI	$0.30^\circ \times 0.22^\circ$ (25 km \times 25 km)	1901–1990	Monthly
15.	<i>Schwarb</i> [2001] <i>Schwarb et al.</i> [2001]	AT, CH, DE, FR, HR, IT, SI	1.25 min \times 1.25 min (1.6 km \times 2.3 km)	1971–1990	Climatology (monthly & annual)
16.	<i>Willmott and Matsuura</i> [2001]	Global	$0.5^\circ \times 0.5^\circ$ (39 km \times 56 km)	1950–1999	Climatology & Monthly
17.	<i>Zierl</i> [2000, 2001]	CH	1 km \times 1 km	1969–1998	Daily
18.	<i>New et al.</i> [2002]	Global	10 min \times 10 min (13 km \times 19 km)	1961–1990	Climatology
19.	<i>Gyalistras</i> [2003]	CH	$0.05^\circ \times 0.05^\circ$ (5 km \times 5 km)	1961–1990 1951–2000	Climatology & Monthly
20.	<i>Gajic-Capka et al.</i> [2003]	HR	700 m \times 700 m	1961–1990	Climatology
21.	<i>Mitchell et al.</i> [2004]	Global	10 min \times 10 min (13 km \times 19 km)	1961–1990 1901–2000	Climatology & Monthly
22.	<i>Schöner</i> [2004]	GAR	$1.0^\circ \times 1.0^\circ$ (77 km \times 111 km)	1800–2003	Monthly
23.	<i>Beck et al.</i> [2005]	Global	$0.5^\circ \times 0.5^\circ$ (39 km \times 56 km)	1951–2000	Monthly

Table 2. Overview of data sets used in this study. The left-hand column numbers indicate the section, where each data set is described; the right-hand column indicates whether each data set was used for the development or the validation of the HISTALP 10-min-grid. The data sets of sections 2.6 and 2.7 refer to the Swiss part of the GAR, whereas the last two data sets (mentioned in Appendix B) to the Austrian and Slovenian parts, respectively.

Section	Short name	Stations / Grid	Temporal Extent	Temporal Resolution	Usage
2.1	HISTALP station-mode	Station-based	1800–2003	Monthly	Development
2.2	ETH climatology	Grid-based	1971–1990	Climatology	Development
2.3	GHCN	Station-based	1971–1990	Monthly	Development
2.3	CRU normals	Station-based	1961–1990	Climatology	Development
2.4	ETH monthly	Grid-based	1901–1990	Monthly	Evaluation
2.5	CRU	Grid-based	1901–2000	Monthly	Evaluation
2.6	MeteoSwiss	Station-based	1961–2000	Monthly	Evaluation
2.7	CHCAM	Grid-based	1951–2000	Monthly	Evaluation
Appendix B	ÖKLIM climatology	Grid-based	1961–1990	Climatology	Evaluation
Appendix B	Slovenian climatology	Grid-based	1961–1990	Climatology	Evaluation

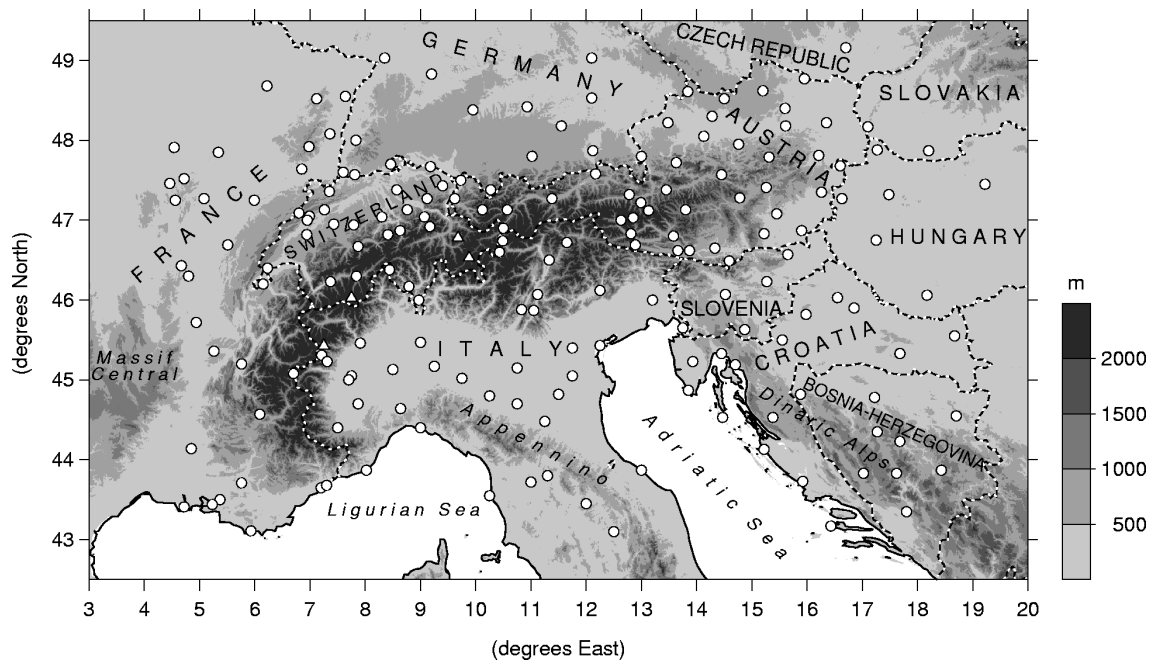


Figure 1. The Greater Alpine Region and the HISTALP station network for precipitation. Low-level (<1500 m) stations are denoted by circles, whereas high-level (>1500 m) stations are denoted by triangles.

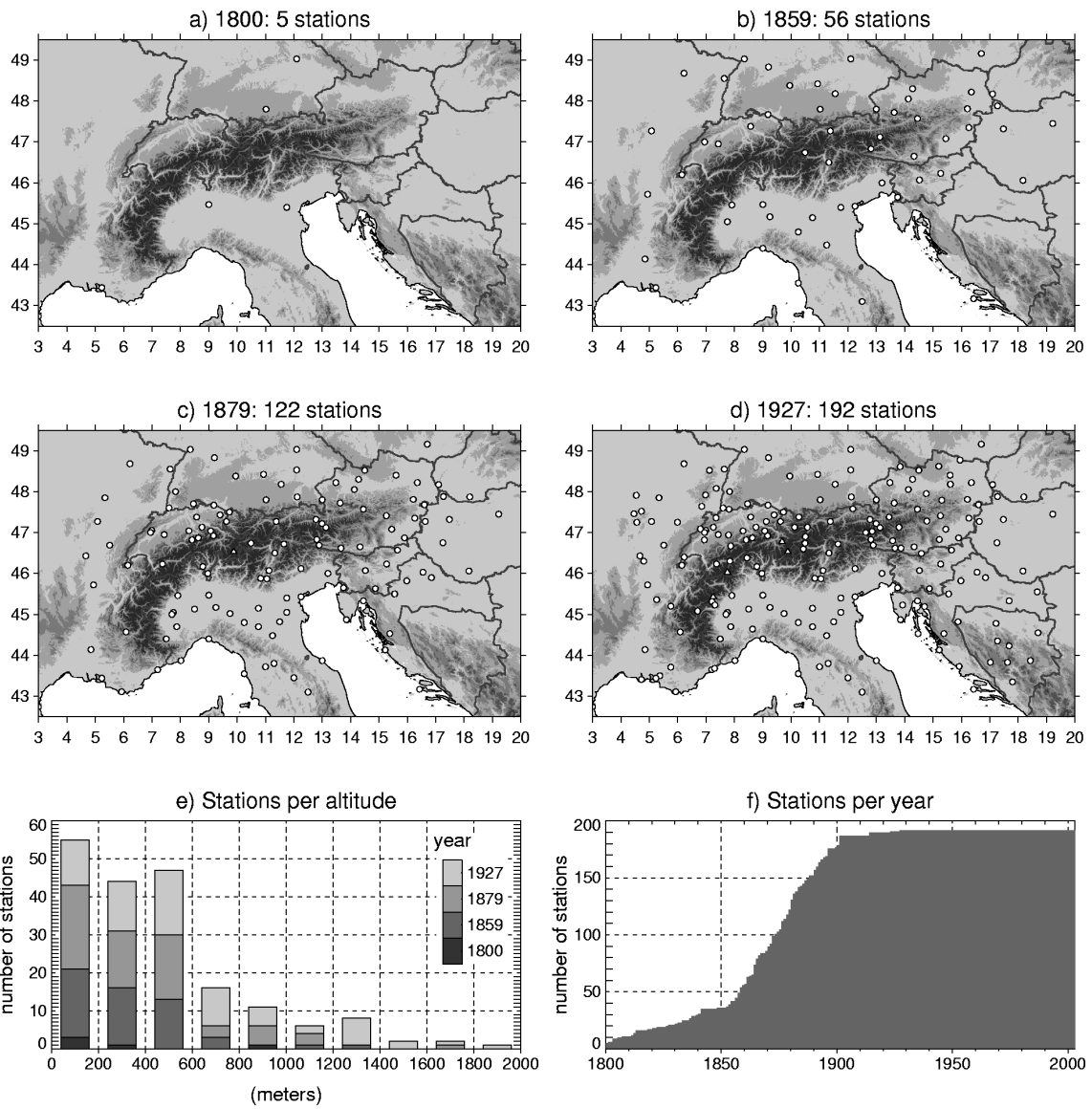


Figure 2. Development of the precipitation data network in the Greater Alpine Region according to availability in the HISTALP data set

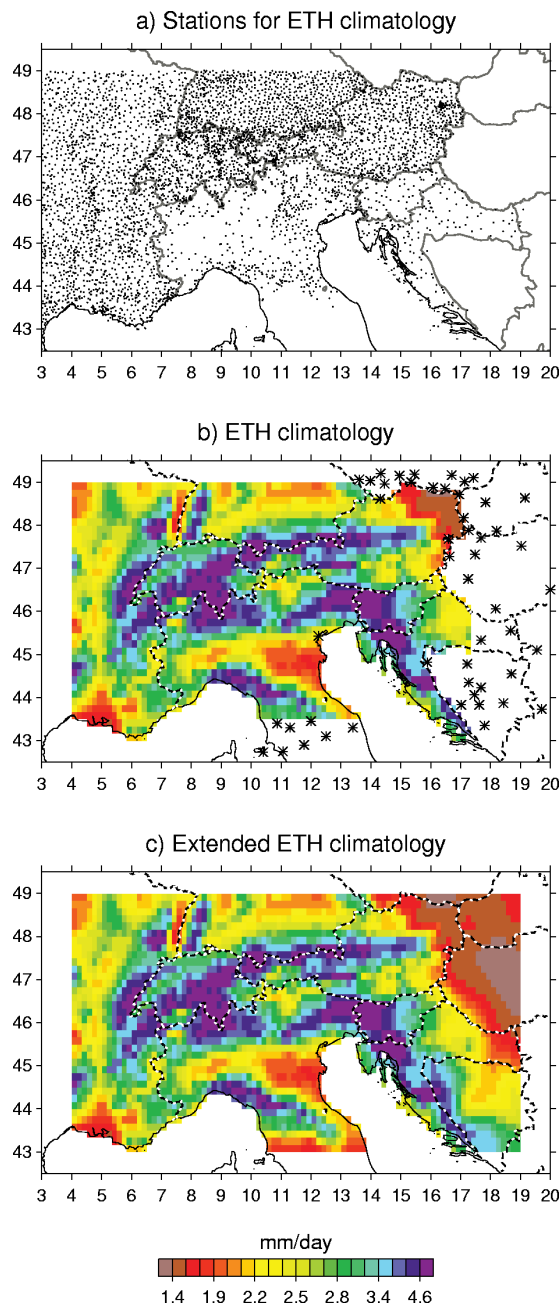


Figure 3. ETH climatology: (a) Location of stations providing data, and (b) the estimated annual-mean precipitation (mm/day) field, for 1971–1990. Also in (b) are shown the station sites (asterisks) whose data were analyzed to extend the climatology to the whole GAR. The geographically-extended climatology (1971–1990) is given in (c).

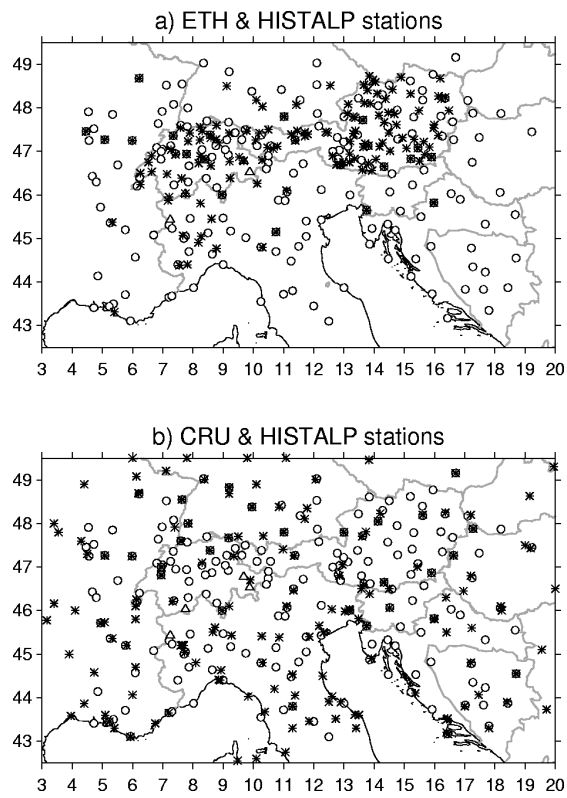


Figure 4. The station networks (denoted with stars) used for the development of (a) the ETH and (b) the CRU monthly precipitation data sets. The HISTALP station network is also overlain (circles/triangles) for comparison.

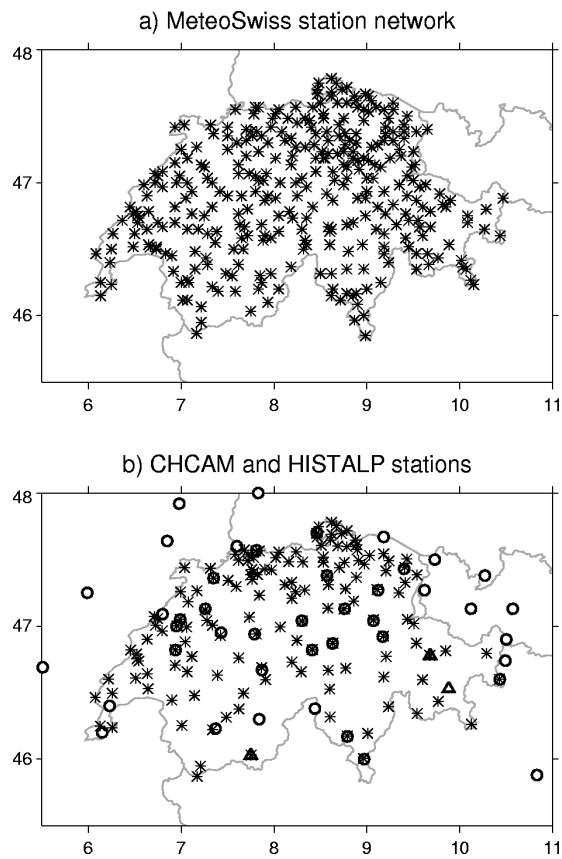


Figure 5. MeteoSwiss station network: (a) the stations used for defining the inverse distance weighting function, shown in Figure 6a, and (b) the stations used for developing the CHCAM data set, overlain with the much sparser HISTALP network (circles/triangles).

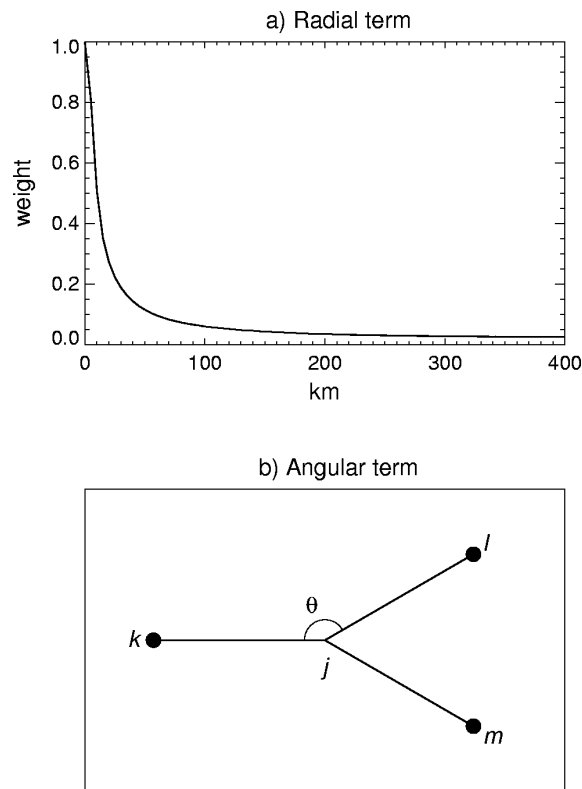


Figure 6. a) The radial term of the ADW interpolation function, and b) Schematic of the definition of angular separation of three stations with respect to grid point j . For the idealized case of equal radial distances of all stations, and with $\theta(k,l)=150^\circ$, $\theta(l,m)=60^\circ$, $\theta(m,k)=150^\circ$, the angular terms are $w_{rad}(k)\sim 0.4$, $w_{rad}(l)\sim 0.3$, $w_{rad}(m)\sim 0.3$.

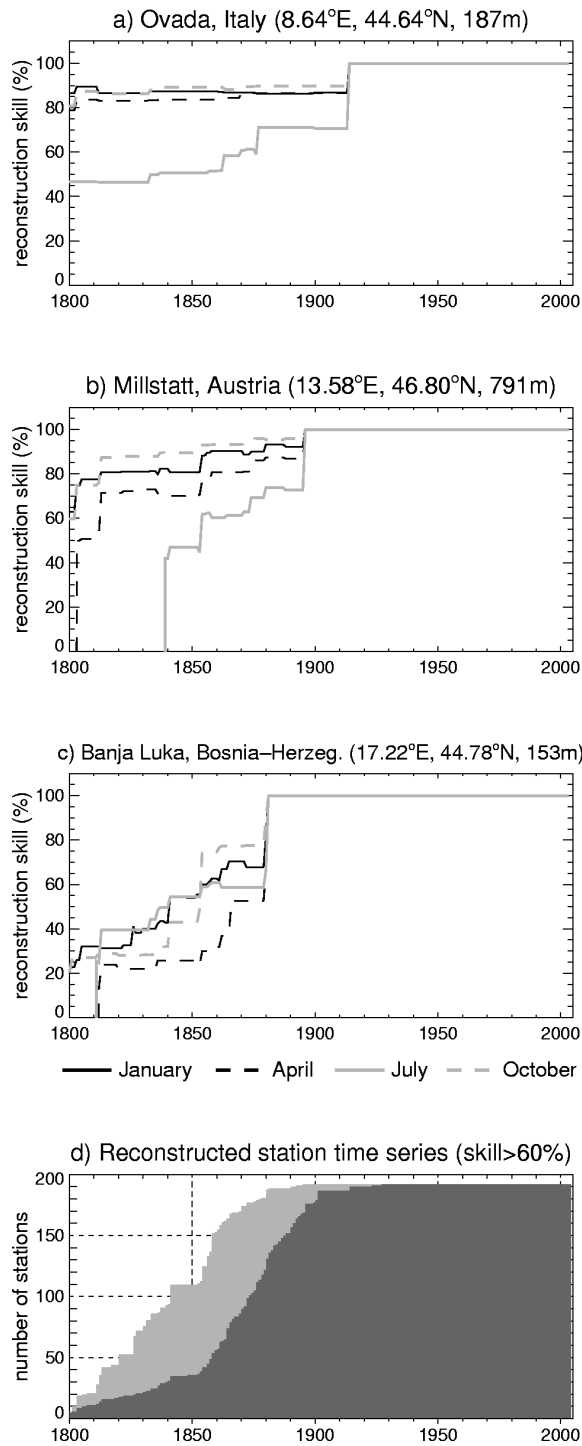


Figure 7. The predicted reconstruction skill (variance explained) for (a) Ovada, (b) Millstatt, and (c) Banja Luka station time series, and (d) the evolution of the number of reconstructed time series (light grey shade) versus the observational series (dark grey shade); only stations with complete (all 12 months) reconstructed monthly values (skill > 60%) are shown in (d).

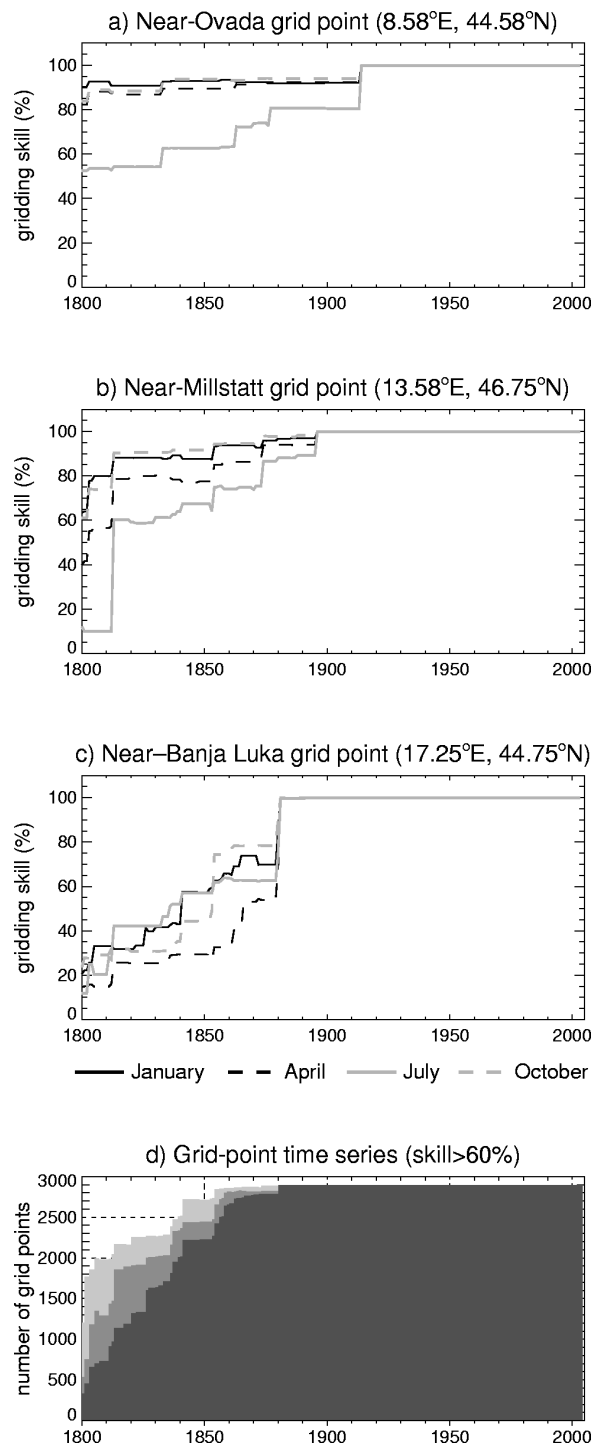


Figure 8. The gridding skill (relative variance-explained score) for grid-point time series located nearby certain station sites: (a) Ovada, (b) Millstatt, and (c) Banja Luka (compare with Figure 7). In the bottom panel (d) the evolution of the number of grid-point time series having skill above 60% for January (light grey), July (moderate grey) and year-round (dark grey) is shown.

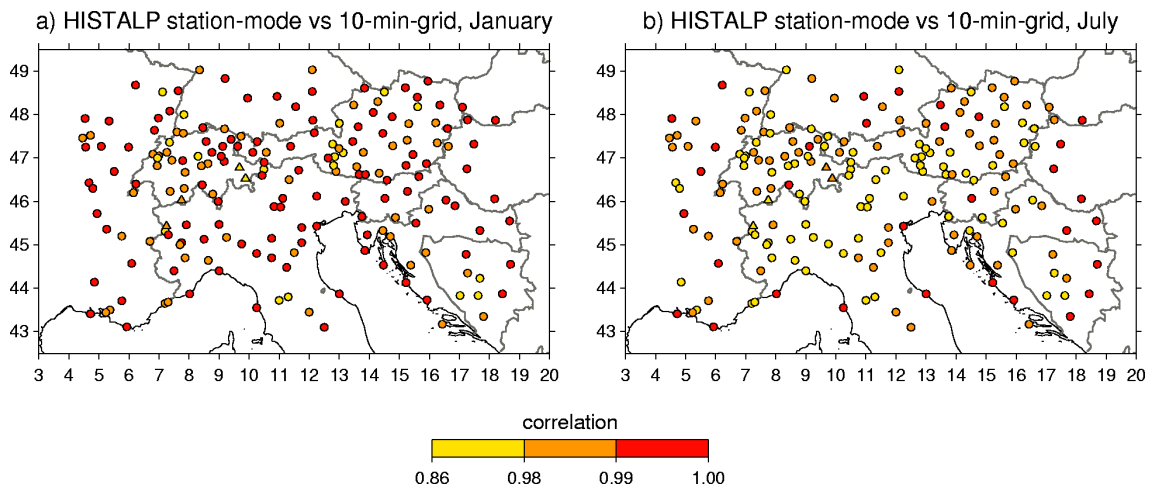


Figure 9. Correlation of the HISTALP 10-min-grid with the HISTALP station-mode data in the 1931–2000 period.

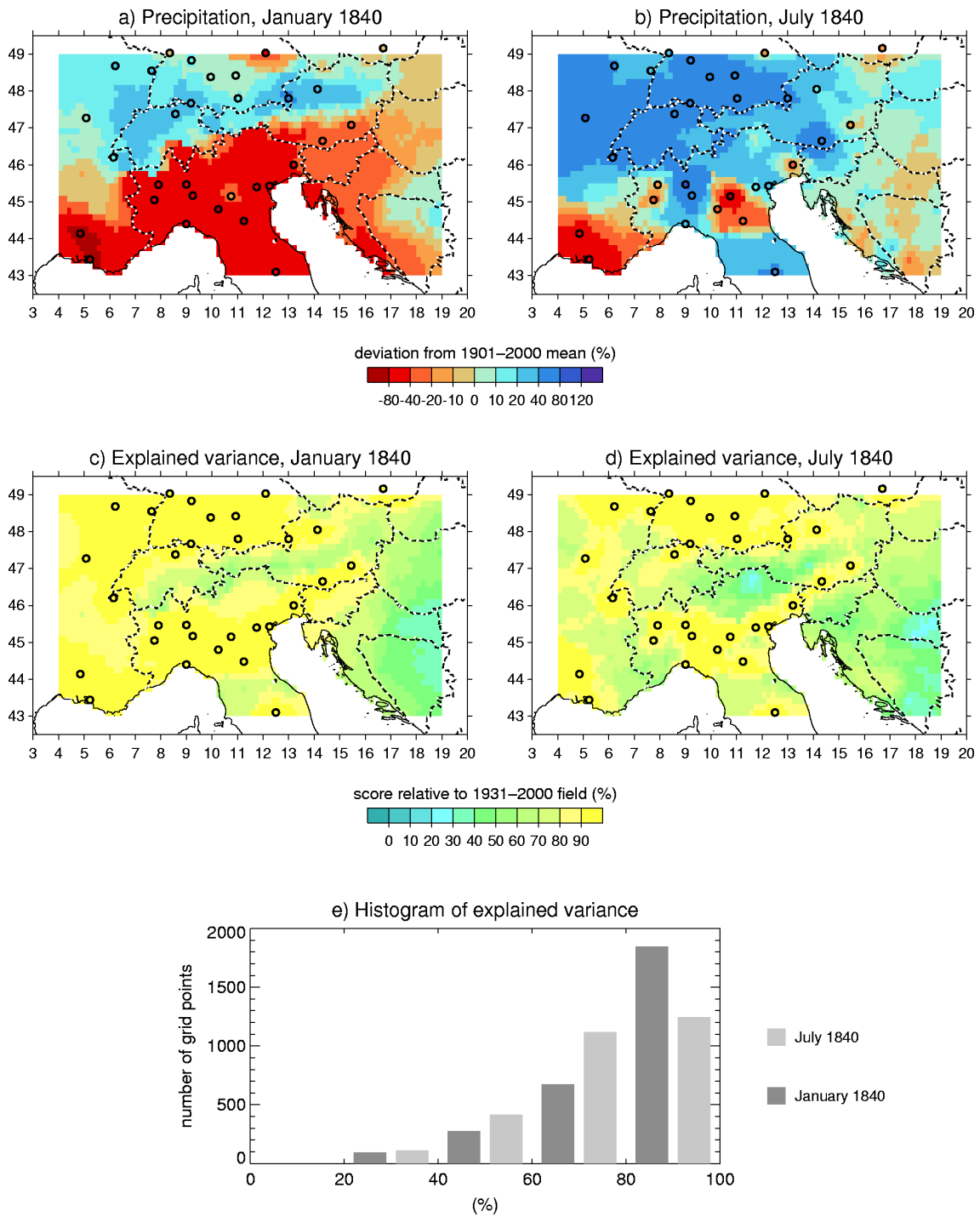


Figure 10. HISTALP 10-min-grid precipitation (overlay with station-mode precipitation, in circles), expressed as per cent anomalies from the 20th century mean, and the associated explained variance, with regard to the 1931–2000 field, for January 1840 (a & c) and July 1840 (b & d). Note the reduction of explained variance score away from the 31 data-providing stations, especially in July, but also over the main Alpine mountain chain. A comparative histogram of explained variance is given in the bottom panel (e).

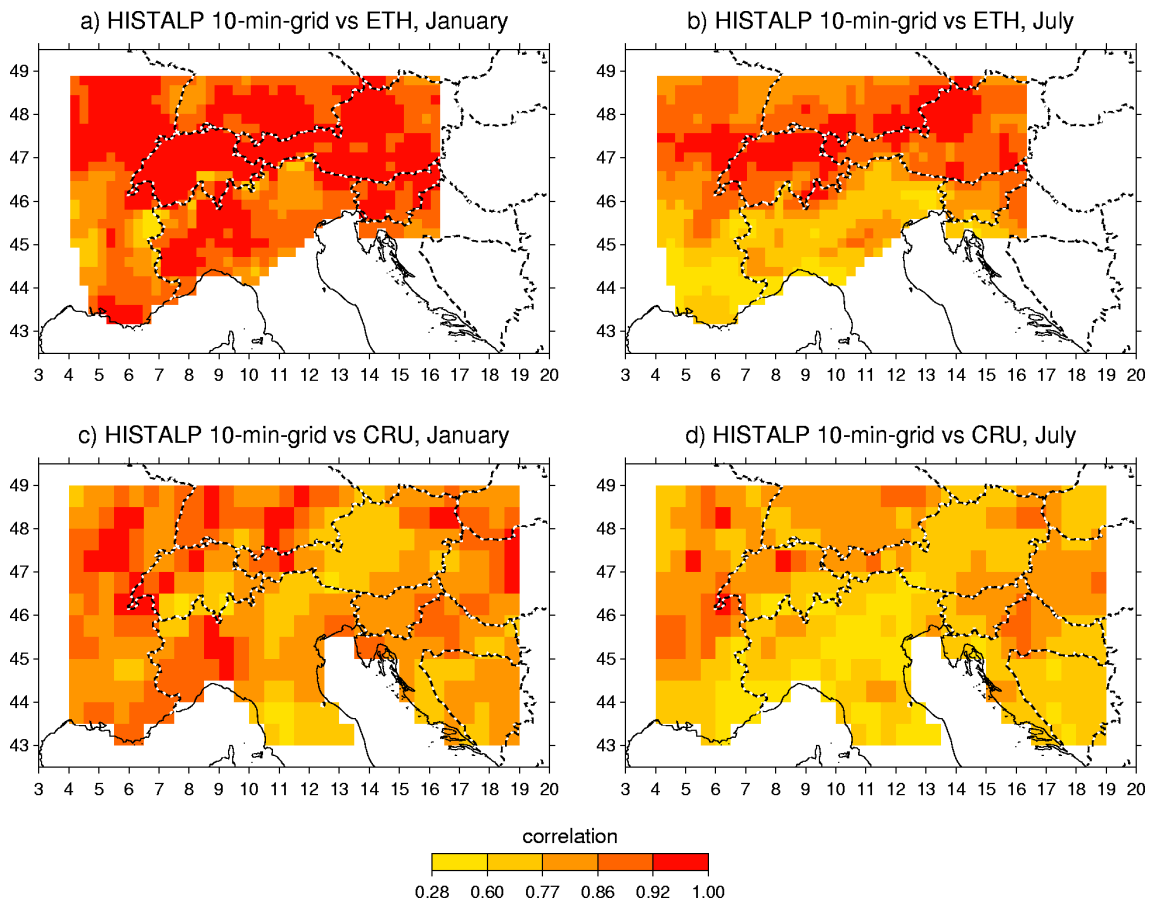


Figure 11. Correlation of HISTALP 10-min-grid with the ETH (a–b) and CRU (c–d) data sets in the 1901–1990 period.

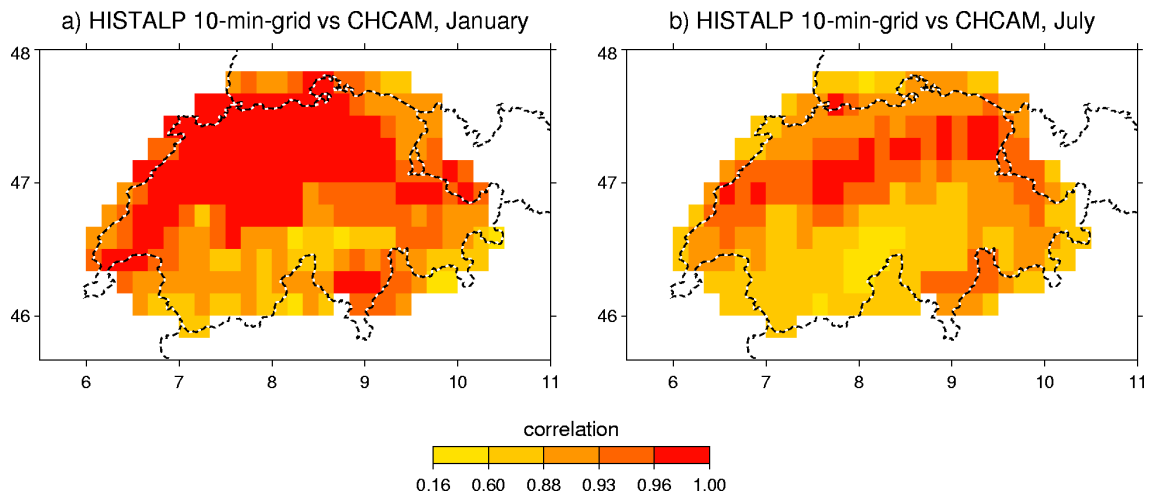


Figure 12. Correlation of HISTALP 10-min-grid with the CHCAM data set (subsamped to 10-min resolution) in the 1951–2000 period.

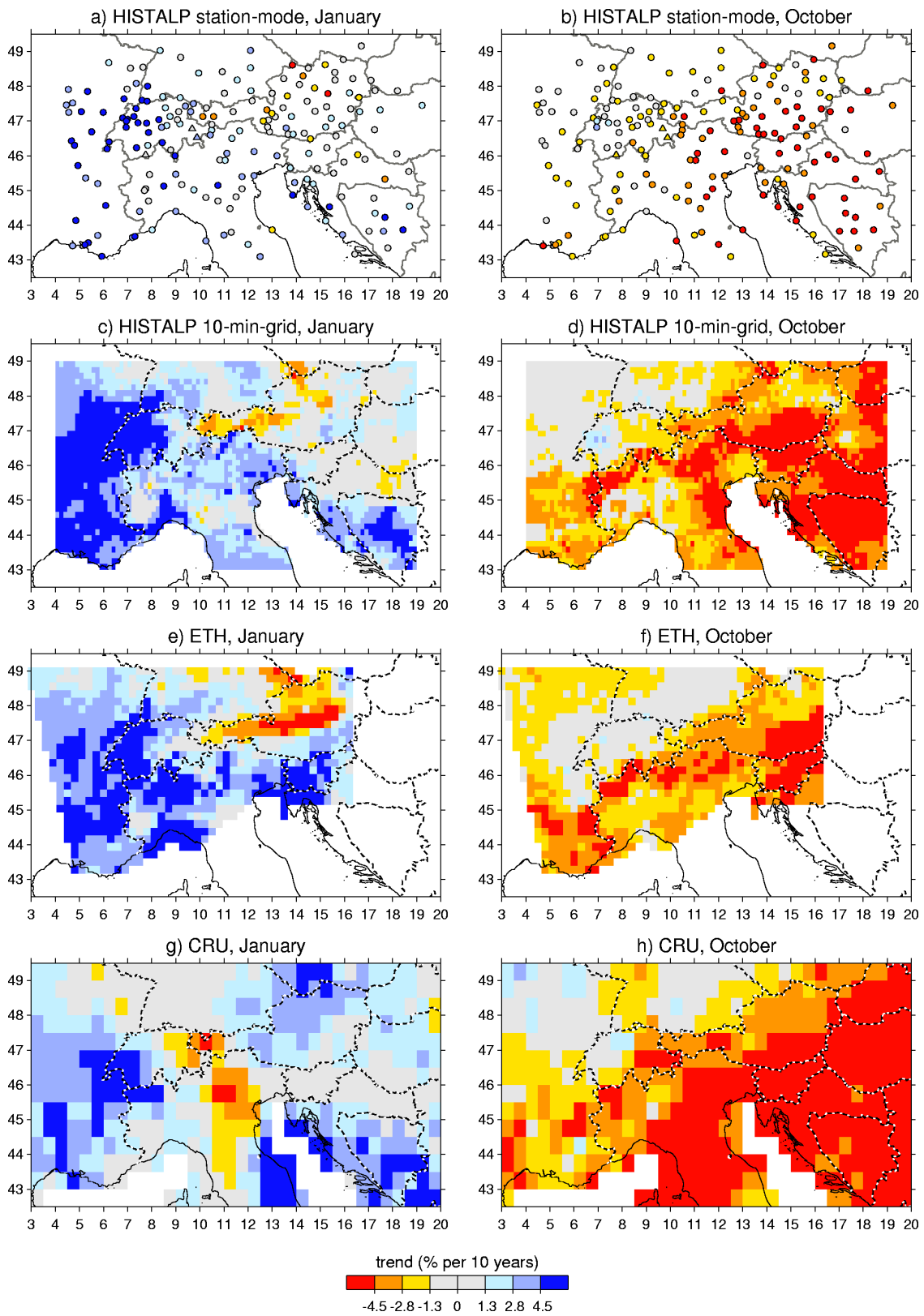


Figure 13. Trends over the 1901–1990 period for January (a, c, d & g) and October (b, d, f & h)

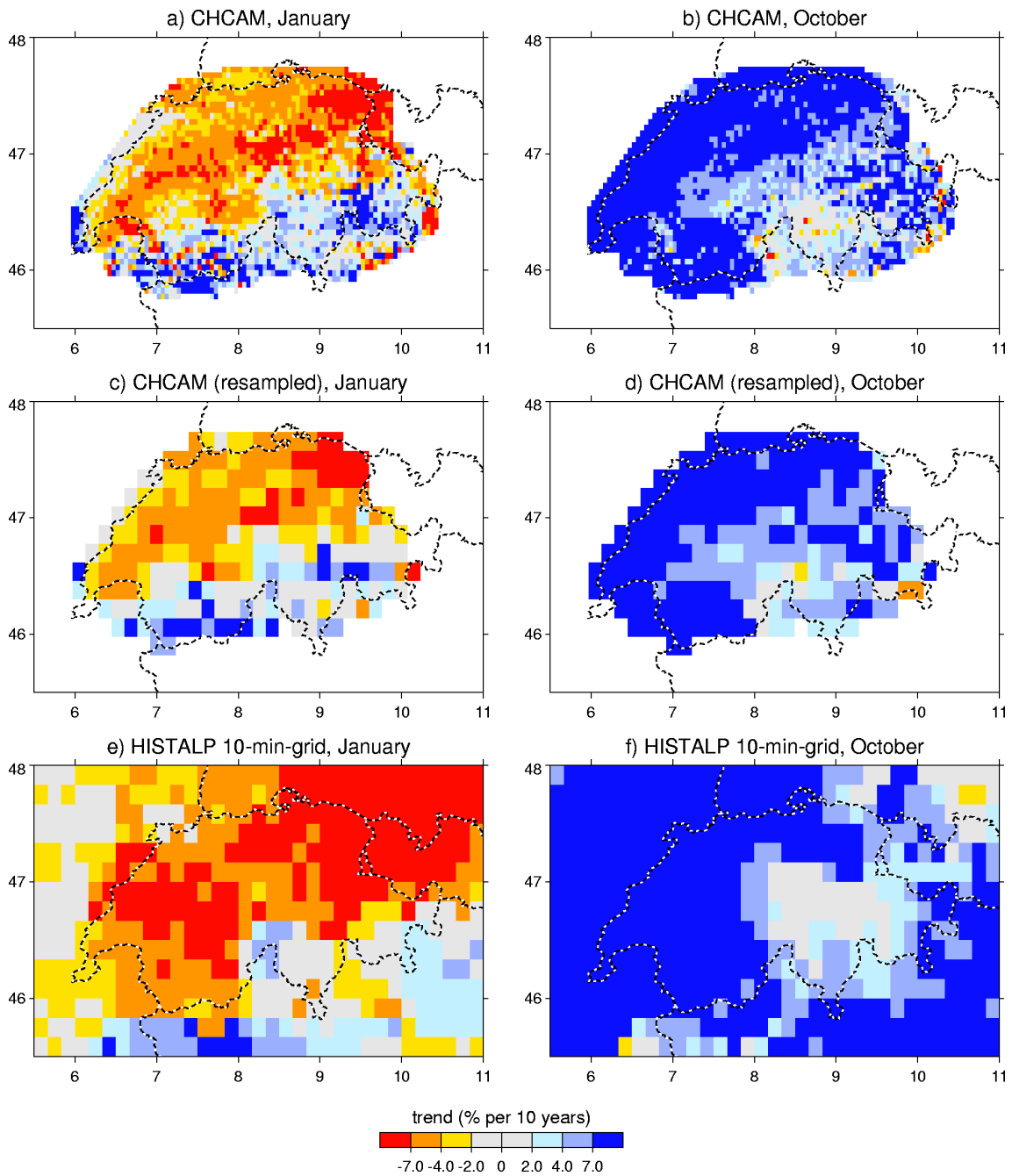


Figure 14. Trends over the 1951–2000 period for January (left-hand panels) and October (right-hand panels), as estimated from the CHCAM and HISTALP 10-min-grid data sets.

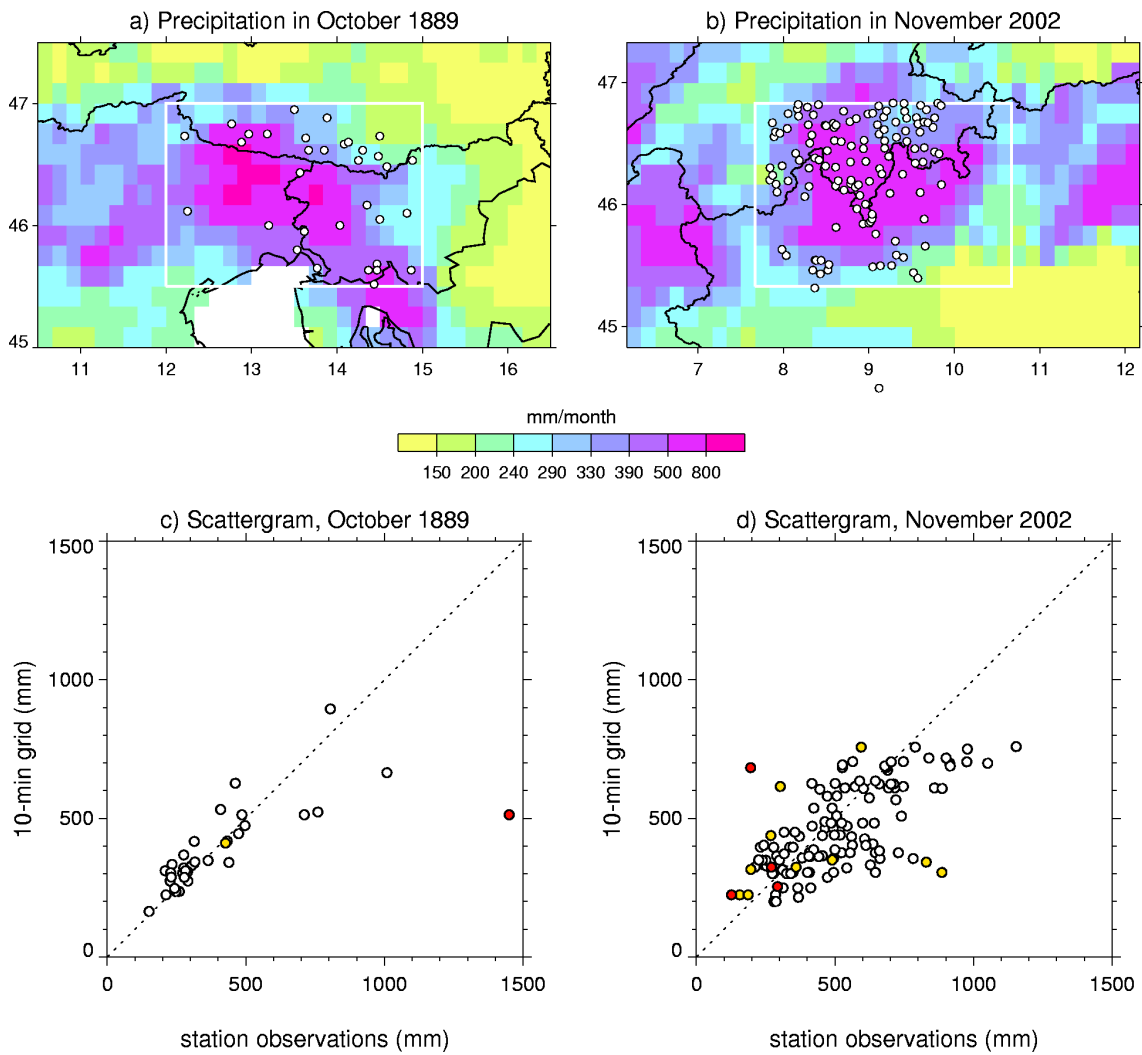


Figure 15. Extreme precipitation months in the GAR, as described by the HISTALP 10-min-grid data set and the geographical position of various collocated station data: a) for October 1889, and b) for November 2002. The respective scattergrams between gridded and station data are given in lower panels (c and d); station data differing more than $\pm 50\%$ and $\pm 100\%$ from neighboring station observations are marked in yellow and red, respectively.

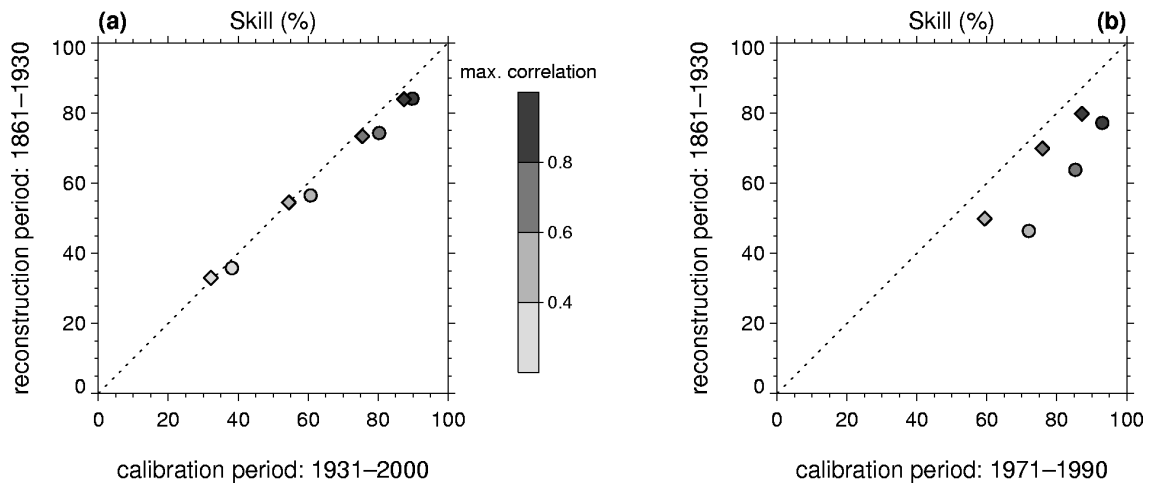


Figure A1. Stability of reconstruction skill within and outside the calibration period using EOFs in comparison to multiple regression. Skill is averaged according to the maximum correlation within the group of the stations selected for reconstruction. EOF-based and multiple regression-based reconstructions are given by diamonds and circles, respectively. Panel (a) corresponds to a 70-year calibration period (as applied in our study), while panel (b) corresponds to a 20-year period

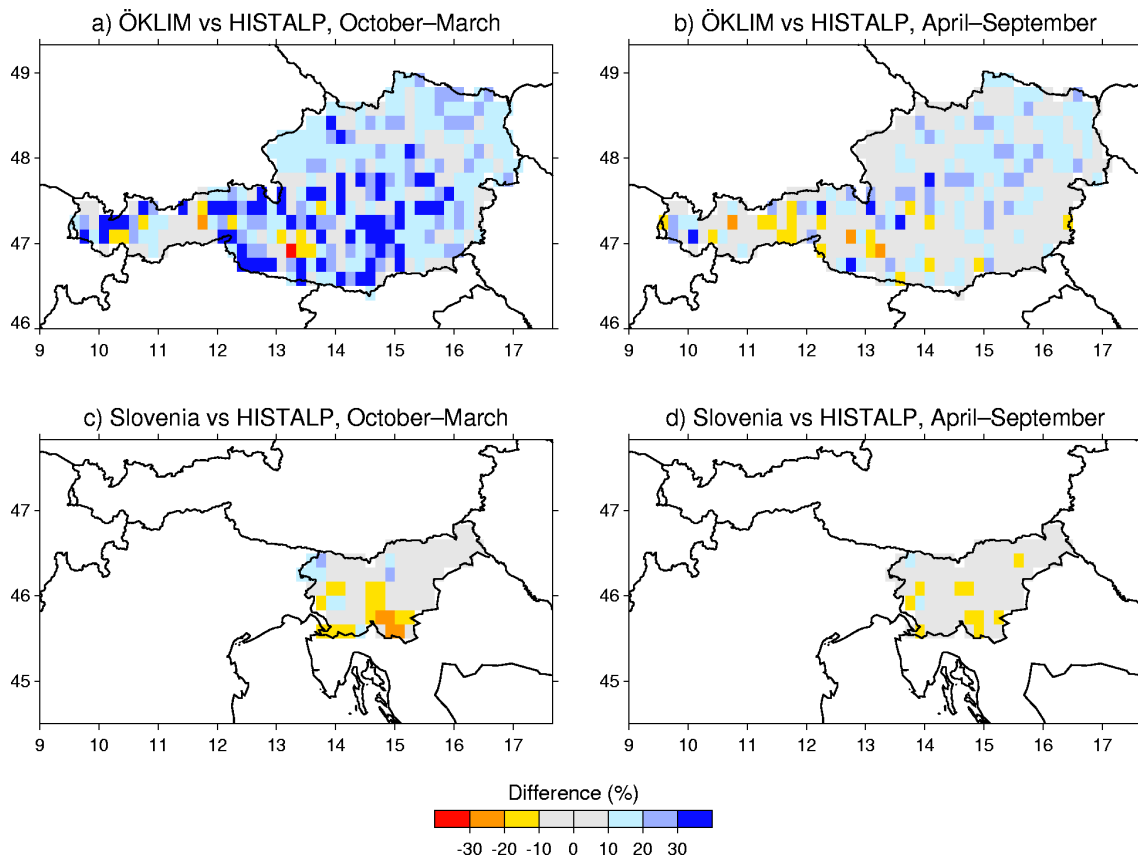


Figure B1. Difference between regional climatologies (1961–1990) minus HISTALP 10-min-grid for winter and summer half-year intervals: ÖKLIM (a–b) and Slovenia (c–d).